MASTER THESIS

Martin Žlábek

Electromagnetic field of non-aligned current loops around the Kerr black hole

Institute of Theoretical Physics

Supervisor of the master thesis: Mgr. David Kofroň, Ph.D.

Study programme: Theoretical physics

Study branch: FTFP

Prague 2024

I declare that I carried out this master thesis independently, and only with the cited sources, literature and other professional sources. It has not been used to obtain another or the same degree.

I understand that my work relates to the rights and obligations under the Act No. 121/2000 Sb., the Copyright Act, as amended, in particular the fact that the Charles University has the right to conclude a license agreement on the use of this work as a school work pursuant to Section 60 subsection 1 of the Copyright Act.

In . . . . date . . . .
Author's signature

i

Title: Electromagnetic field of non-aligned current loops around the Kerr black hole

Author: Martin Žlábek

Institute: Institute of Theoretical Physics

Supervisor: Mgr. David Kofroň, Ph.D., Institute of Theoretical Physics

Abstract:

This work discusses electromagnetic fields around Kerr black hole. We extend prior work by finding a new source term - a non-axial current loop. We analyze this solutions behaviour. We also discuss in detail the Meissner effect. Explore various visualization techniques of electromagnetic fields and we also show that the electromagnetic invariants vanish at the horizon under the same conditions that trigger the Meissner effect.

Keywords:

general relativity, Kerr black hole, electrodynamics, current loop, Meissner effect

Název Práce: Elekromagnetické pole skloněné proudové smyčky na pozadí Kerrovy černé díry

Autor: Martin Žlábek

Ústav: Ústav teoretické fyziky

Vedoucí diplomové práce: Mgr. David Kofroň, Ph.D., Ústav teoretické fyziky

Abstrakt:

Tato práce se zabývá elektromagnetickými poli v okolí Kerrovy černé díry. Rozšiřujeme předchozí práci o nový zdrojový člen - neaxiálně symetrickou proudovou smyčku. Zkoumáme chování tohoto řešení. Podrobně se zabýváme také Meissnerovým jevem. Zkoumáme různé techniky vizualizace elektromagnetických polí a také ukazujeme, že elektromagnetické invarianty jsou nulové na horizontu za stejných podmínek, které vyvolávají Meissnerův jev.

Klíčová slova:

obecná teorie relativity, Kerrova černá díra, elektrodynamika, proudová smyčka, Meissnerův jev

Contents

Introduction

The Kerr spacetime, discovered in 1963 by Roy Kerr is one of the most important solution's of Einstein's equations. It describes the geometry surrounding a rotating black hole. Black holes are widely accepted by the scientific community as real physical objects. Recent observations suggesting existence of black holes with large rotational parameter a [1] bolster the importance of the Kerr solution.

One of crucial aspect of understanding the observations of black holes lies in understanding behaviour of electromagnetic field around these objects. These fields play a vital role in various phenomena like jets and accretion disks. The electromagnetic field interacts with the underlying geometry in a fascinating and non-trivial way. For example the rotation can induce electric fields from purely magnetic fields and vice-versa.

A important consequence of this interaction lies in the Meissner-like effect. The Meissner effect is usually understood as the expulsion of magnetic field lines from a superconductor once its cooled below the critical temperature T_c. In Kerr spacetime a similar Meissner-like effect was discovered, where the flux of any stationary axially symmetric electromagnetic fields across the rotating black hole horizon goes to zero when the black hole becomes extremal i.e. when it's rotational parameter a is equal to the mass of the black hole M.

This thesis leverages the so-called Newman-Penrose (NP) formalism. A formalism that reformulates the traditional tensorial expression in general relativity into complex forms, it turns out that such a formalism allows one to perform perturbations of the metric tensor in an elegant way. We build upon the work of J. Bičák and L. Dvořák [2], who found the solution of arbitrary stationary electromagnetic test field in Kerr spacetime with the source located outside of the black hole, by to deriving a new source — a non-axial current loop. Such complex source should offer valuable insight into the intricate interaction of the test field and the geometry. We also explore the Meissner effect, proving that non-only the the flux vanishes for the extreme black hole in the axially symmetric case, but also both invariants of electromagnetic field vanish.

Before presenting these results we briefly summarize the NP formalism, the results of J. Bičak and L. Dvořák and any necessary mathematical tools.

1. GR preliminaries

General relativity was introduced more than a hundred years ago by Albert Einstein. Unlike in Newtonian theory, where the background is a fixed Euclidean space (R^3) with a separate time parameter (R), and gravity is treated as a force acting on this manifold, general relativity relativity combines spacetime into a four-dimensional Lorentzian manifold (M^4). Gravity is then understood as the curvature of spacetime itself, caused by the distribution of energy and matter in the system.

Mathematically, the curvature in Einstein's theory is described by the Einstein field equations, in geometrized units where the speed of light in vacuum c and the gravitational constants G are set to unity, the Einstein field equations are

$$R_{\mu\nu} - \frac{1}{2}R g_{\mu\nu} + \Lambda g_{\mu\nu} = 8\pi T_{\mu\nu}. \tag{1.1}$$

Here, $R_{\mu\nu}$ represents the Ricci curvature tensor, R is the Ricci scalar, $g_{\mu\nu}$ is the metric tensor that describes the geometry of spacetime, Λ is the cosmological constant, and $T_{\mu\nu}$ is the stress-energy tensor representing the distribution of energy and matter.

The stress-energy tensor $T_{\mu\nu}$ describes the energy density, momentum density, and pressure of the matter and non-gravitational fields present in the system. If we consider consider an electromagnetic source, described by the current density tensor J^μ and governed by the Maxwell equations

$$\begin{aligned}
\nabla_\mu F^{\mu\nu} &= 4\pi J^\nu, \\
F^{[\alpha\beta;\gamma]} &= 0.
\end{aligned} \tag{1.2}$$

The stress-energy tensor for an electromagnetic field can then be written as

$$T_{\mu\nu} = \frac{1}{4\pi}\left(F_{\mu\iota}F^\iota{}_\nu - \frac{1}{4}g_{\mu\nu}F_{\iota\kappa}F^{\iota\kappa} \right). \tag{1.3}$$

In general relativity, as in any field of physics, symmetries play an important role. Symmetries are described by Killing vectors, which are vector fields that satisfy the Killing equation

$$\mathcal{L}_\xi g_{\mu\nu} = \xi_{\mu;\nu} + \xi_{\nu;\mu} = 0. \tag{1.4}$$

Intuitively, this equation says that the metric is unchanged under the action of the Killing field or in other words, the symmetries described by Killing vectors are such that the geometry of spacetime remains invariant.

1.1 Kerr Metric

In 1963, Roy Kerr discovered the so-called Kerr metric which depicts the space-time geometry surrounding a rotating black hole asymptotically approaching flat spacetime. This solution is determined by just two quantities, the black hole mass M and the rotational parameter a, which is just the angular momentum divided by mass $a = J/M$.

It's important to note that there exist no Birkhoff theorem for rotating black holes. Which states that any spherically symmetric vacuum solution of the Einstein equations (1.1) must necessarily be the Schwarzschild solution. Thus "it is not true that the spacetime geometry in the vacuum region outside a generic rotating star (or planet) is a part of the Kerr geometry. The best result one can obtain is the much milder statement that outside a rotating star (or planet) the geometry asymptotically approaches the Kerr geometry". [3].

The metric takes a relatively simple form in the Boyer-Lindquist coordinates

$$ds^2 = -\left(1 - \frac{2Mr}{\Sigma}\right)dt^2 - \frac{4Mar\sin^2\theta}{\Sigma}dtd\varphi + \frac{\Sigma}{\Delta}dr^2 + \Sigma d\theta^2 + \frac{A\sin^2\theta}{\Sigma}d\varphi^2, \quad (1.5)$$

where

$$\Delta = r^2 - 2Mr + a^2,$$
$$\Sigma = r^2 + a^2\cos^2\theta,$$
$$A = (r^2 + a^2)^2 - \Delta a^2\sin^2\theta = 2Mr(r^2 + a^2) + \Delta\Sigma.$$

The Kerr metric is *stationary*: it has a Killing vector field that is timelike at infinity, and the metric is *axisymmetric*: it has a Killing vector field which has closed spacelike trajectories. These two commuting Killing vector fields are

$$t^\mu = \frac{\partial x^\mu}{\partial t}, \quad \varphi^\mu = \frac{x^\mu}{\partial\varphi}. \quad (1.6)$$

For $a \to 0$ the Boyer-Lindquist line element reduces to the Schwarzschild whereas for $M \to 0$ (while keeping a constant) the line element reduces to Minkowski's line element in oblate spheroidal coordinates.

The metric components have singularities at

$$\Sigma = 0 \iff r^2 + a^2\cos^2\theta = 0 \implies r = 0 \wedge \theta = \frac{\pi}{2}, \quad (1.7)$$

$$\Delta = 0 \iff 1 - \frac{2m}{r} + \frac{a^2}{r^2} = 0 \implies r = r_\pm = M \pm \sqrt{M^2 - a^2}. \quad (1.8)$$

The first corresponds to a real physical curvature since the Kretschmann invariant K diverges,

$$K \equiv R_{\alpha\beta\gamma\iota}R^{\alpha\beta\gamma\iota} = \frac{48M^2}{\Sigma^6}\left(r^2 - a^2\cos^2\theta\right)\left(\Sigma^2 + 16r^2\cos\theta(r^2 - \Sigma)\right). \quad (1.9)$$

The $\Delta = 0$ surface are null hypersurfaces. Forming the horizons of the black hole usually called the outer r_+ and inner r_- horizon. The coefficient g_{tt} in the metric (1.5) changes sign on the spacelike surfaces $r_{0,1}$ where

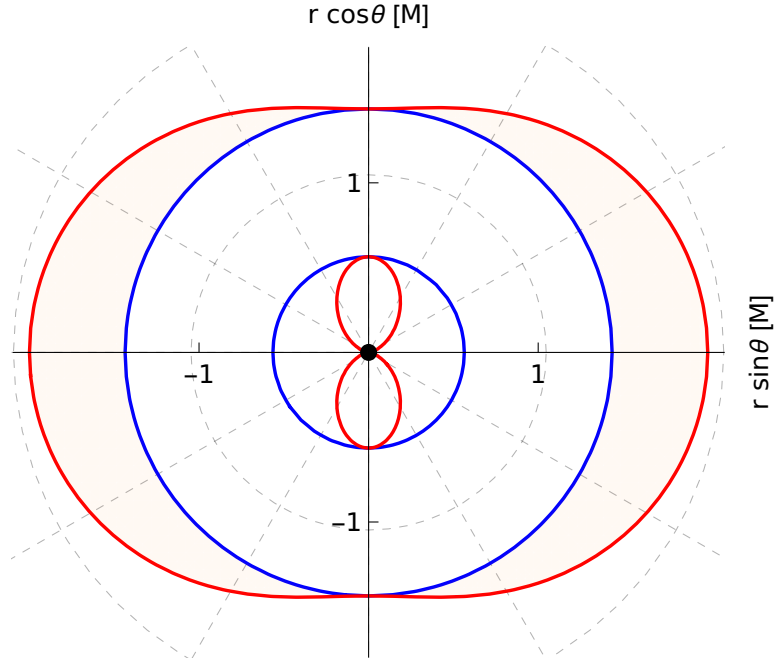$$r_{0,1} = M \pm \sqrt{M^2 - a^2\cos^2\theta}. \quad (1.10)$$

Figure 1.1: subsection of Kerr spacetime with $a = 9/10$ in units of Mass. Static limits are red and event horizons are blue. The ergoregion is colored opaque red.

The outer surface where $r = r_1$ is the surface of infinite redshift since $g_{tt} = g_{\mu\nu}t^\mu t^\nu = 0$. The outer/inner horizons and the outer/inner event horizons coincide at the poles where $\theta = 0, \pi$. In the region $r_+ < r < r_1$ the coordinates t and r are both spacelike but it is still possible to escape to infinity, this region is called the *ergoregion*. For the case of extremal black hole $a \to M$ the two horizons coincide $r_+ = r_- = M$. Furthermore $a \geq M$ the black hole singularity becomes *naked*. Since there exist no reals roots of (1.8), this means that no horizons are present. Usually while not taking in mind theories like quantum loop theory the naked singularities are thought to be non-physical since they, among others, violate causality.

As we can see from (1.8) and (1.10), for the Schwarzschild case $a \to 0$ there is just one horizon for outside of the coordinate singularity and surface $\Delta = 0$ also becomes the surface of infinite redshift.

Eddington-Finkelstein-type coordinates

The Boyer-Lindquist coordinates (1.5) do not behave nicely near the horizons. For an infalling photon or test particle the coordinate time $t \to \infty$ as $r \to r_+$, exactly as in the Schwarzschild case. Moreover, an infinite twisting of worldlines around the horizon happens since $\varphi \to \infty$ [4]. To alleviate these problems we can introduce Eddington-Finkelstein-type coordinates. Introducing an advanced null coordinate v and a new angular coordinate ψ such that

$$dv = dt + \frac{r^2 + a^2}{\Delta}dr, \quad d\psi = d\varphi + \frac{a}{\Delta}dr. \tag{1.11}$$

The metric (1.5) takes a new form in these coordinates

$$ds^2 = -\left(1 - \frac{2Mr}{\Sigma}\right)(\mathrm{d}v - a\sin^2\theta\,\mathrm{d}\psi)^2$$
$$+ 2(\mathrm{d}v - a\sin^2\theta\,\mathrm{d}\psi)(\mathrm{d}r - a\sin^2\theta\mathrm{d}\psi) + \Sigma(\mathrm{d}\theta^2 + \sin^2\theta\,\mathrm{d}\psi^2). \tag{1.12}$$

Such a form of the metric is clearly non-singular at $\Delta = 0$.

Doran Coordinates

Relatively recently Doran [5] introduced a new form of the Kerr metric. This form is particularly well adapted for analyzing the motion of free-falling time-like observers. Making it useful for studying physical phenomena around rotating black hole. The coordinates are also chosen such that the solution is well behaved at the horizon unlike the Boyer-Lindquist coordinates. Consider the coordinate transformation

$$\mathrm{d}\tilde{t} = \mathrm{d}t + \frac{\sqrt{2Mr(r^2 + a^2)}}{\Delta}\mathrm{d}r,$$
$$\mathrm{d}\tilde{\varphi} = \mathrm{d}\varphi + \frac{a\sqrt{2Mr}}{\sqrt{r^2 + a^2}\Delta}\mathrm{d}r. \tag{1.13}$$

Then the line element (1.5) takes the form

$$ds^2 = -\mathrm{d}\tilde{t} + \frac{\Sigma}{r^2 + a^2}\left[\mathrm{d}r + \frac{\sqrt{2Mr(r^2 + a^2)}}{\Sigma}\left(\mathrm{d}\tilde{t} - a\sin^2\theta\mathrm{d}\tilde{\varphi}\right)\right]^2$$
$$+ \Sigma\mathrm{d}\theta^2 + (r^2 + a^2)\sin^2\theta\mathrm{d}\tilde{\varphi}. \tag{1.14}$$

Clearly, such coordinates are regular at the horizon $\Delta = 0$. For the vacuum case $a \to 0, M \to 0$ we recover the Minkowski metric with spherical coordinates.

1.1.1 Embedding

Visualizing general relativistic solutions poses at least two major hurdles: first, we're not just dealing with three-dimensional space, but with the four-dimensional space and time. Second, this spacetime is often described using specific coordinates, which can mislead us and make it difficult to understand its true shape. One of the more useful visualization is the use of embedding diagrams. Such diagrams are created by choosing a surface and embedding this surface into a flat-space metric. Such has been explored in [6].

Consider a 2D sub-manifold $M^{r\theta}$, defined by taking $t = \text{const.}$, $\varphi = \text{const.}$, of the 4D manifold Kerr manifold M with the metric line element in Boyer-Lindquist coordiantes (1.5). Taking the part of spacetime outside the outer horizon we get the induced line element

$$d\sigma^2 = \Sigma\left(\frac{\mathrm{d}r^2}{\Delta} + \mathrm{d}\theta^2\right), \tag{1.15}$$

since (1.15) is independent of t and φ, the sub-manifold is the same for any value of t, φ and thus has the same intrinsic geometry. We further consider the
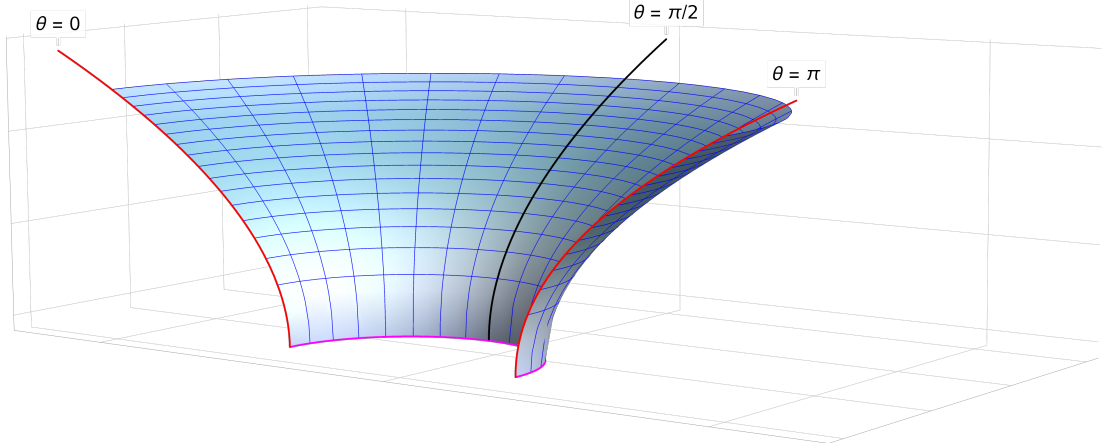
Figure 1.2: Embedding of $M_\Omega^{r\theta}$ in $\mathbb{R}^3$ for $a = 1/2$ using the Boyer-Lindquist coordinates. With highlighted curves of constant θ and r. The horizon r_+ is magenta.

conformal transformation of the manifold $M^{r\theta} \to M_\Omega^{r\theta}$ defined by

$$d\sigma_\Omega^2 = \Omega^2 d\sigma^2 = \Omega^2 \frac{\Sigma}{r^2}\left(\frac{r^2 dr^2}{\Delta} + r^2 d\theta\right), \quad \Omega^2 = \frac{r^2}{\Sigma}. \tag{1.16}$$

Since this is a conformal transformation, the angle of intersection of any curve is the same in $M^{r\theta}$ as in $M_\Omega^{r\theta}$. We further consider the embedding of $M_\Omega^{r\theta}$ in $\mathbb{R}^3$, we choose cylindrical coordinates (z, R, Θ), the line elements are then related by

$$\frac{r^2 dr^2}{\Delta} + r^2 d\theta^2 = dz^2 + dR^2 + R^2 d\Theta. \tag{1.17}$$

Taking $z = z(r)$ and $R = R(r)$ we get the set of equations

$$R(r)^2 = r^2,$$
$$\left(\frac{dz(r)}{dr}\right)^2 = \frac{r^2}{\Delta} - \left(\frac{dR(r)}{dr}\right)^2. \tag{1.18}$$

One of the solutions of this is

$$z(r') = \int_{r_+}^{r'} \sqrt{\frac{r^2 - \Delta}{\Delta}} dr. \tag{1.19}$$

Such an integral is always positive and well defined above the outer horizon. It can be explicitly solved in terms of elliptic integrals. For the Schwarzschild case we recover

$$z(r)_{a=0} = 2\sqrt{2}M\sqrt{\frac{-2Mr + r^2}{Mr}}. \tag{1.20}$$

The embedding can be seen in Fig. 1.2. For the extremal case $r \to r_+, a \to M$ the function $z(r) \to -\infty$, so that the horizon is moved to logarithmic infinity. We embedded the part of the metric for which $r > r_+$. The whole slices of the metric $t = const., \varphi = const.$ (1.5) cannot be embedded [7]. This is because the Gaussian curvature changes sign in the Kerr metric. For the same reason it is

not possible to embed the metric in the Doran coordinates (1.14) even thought there is no coordinate singularity. We've explicitly provided the embedding of the $t = const., \varphi = const.$ space, the procedure for embedding $t = const. \theta = const.$ is completely analogous.

2. Tetrad Formalism

Sometimes, instead of dealing with a local coordinate basis, it is useful to proceed by choosing a suitable tetrad basis of four linearly independent vector-fields. We can then project relevant quantities on this chosen basis.

We will now introduce two formalism which we will later utilise: (a) the NP formalism: which is useful for many calculations in GR, (b) the observer tetrad formalism: which is useful to relating quantities in GR to actually measurable quantities. Before that we quickly introduce general tetrad formalism. A more exhaustive a rigorous introduction can be found in [8].

A tetrad basis is composed of four linearly independent vector-fields chosen ideally to represent underlying symmetries of space-time. First we need to define the tetrad basis. Consider four linearly independent vectors

$$e_{(a)}{}^j, \quad a = 0, 1, 2, 3. \tag{2.1}$$

We have introduced new set of (tetrad) indices which are distinguished by being in parentheses.

The associated covariant vectors to (2.1) are

$$e_{(a)j} = e_{(a)}{}^j g_{ij}. \tag{2.2}$$

The tetrad indices behave as normal indices but they form a different basis

$$\eta_{(a)(b)} e^{(a)}{}_j = e_{(b)j}, \quad \eta^{(a)(b)} e_{(a)j} = e^{(a)}{}_j. \tag{2.3}$$

We assume that the matrix $\eta_{(a)(b)}$ is constant. We also define the inverse relation as

$$e^i_{(a)} e^{(b)}_i = \delta^{(b)}_{(a)}, \quad e^i_{(a)} e^{(a)}_j = \delta^i_j. \tag{2.4}$$

It is clear that any tensor can be projected onto the tetrad frame as

$$T_{(a)(b)(c)\dots}{}^{(\mu)(\nu)(\zeta)\dots} = e_{(a)}{}^i e_{(b)}{}^j e_{(c)}{}^k \dots e^{(\mu)}{}_m e^{(\nu)}{}_n e^{(\zeta)}{}_o \dots T_{ijk\dots}{}^{mno\dots}. \tag{2.5}$$

We also define derivatives as

$$A_{(a),(b)} = e_{(a)}{}^j A_{j;l} \, e_{(b)}{}^i + e_{(c)}{}^k e_{(a)k;i} \, e_{(b)}{}^i A^{(c)}. \tag{2.6}$$

This equation can be rewritten as

$$A_{(a),(b)} = e_{(a)}{}^j A_{j;l} \, e_{(b)}{}^i + \gamma_{(c)(a)(b)} A^{(c)}, \tag{2.7}$$

where the definition of $\gamma_{(a)(b)(c)}$ called *Ricci rotation-coefficients* is clear from comparison of equations (2.6) and (2.7).

2.1   Observer tetrad formalism

Let us first agree on convention for the observer tetrads, instead of numbering the tetrad indices with numbers $a = 0, 1, 2, 3$ we will when possible denote the

indices with appropriate coordinate symbols, this has the added advantage of telling us against which basis we're expressing the tensor. Thus for expression in Boyer-Lindquist coordinates the indices take the values $a = t, r, \theta, \phi$.

As mentioned above sometimes the choice of a tetrad can simplify the problem, but this it's not it's only application. If we want to relate covariant quantities to actually measurable quantities we need to consider a family of *physical observers* — a congruence of time-like world-lines with a tangent four-velocity field of the observer $e^\mu_{(0)} = u^\mu$, with $u^\mu u_\mu = -1$, and a suitable orthonormal spatial bases $\{e^\mu_{(i)}\}_{i=1,2,3}$. In such a physical tetrad the metric locally takes the form

$$\eta_{\mu\nu} = \text{diag}(-1, 1, 1, 1). \tag{2.8}$$

The choice of tetrad is up to us, but the only sensible tetrad are the ones which represent some kind of possibly real physical observer. After that we usually choose the tetrad is the manner so that they represent the physical properties of the system or can be written simply in some convenient coordinates so that the resulting expression are not too complicated.

ZAMO

A somewhat common choice of an observer tetrad in Kerr spacetime this is the zero angular momentum observers (ZAMO) tetrad. Such observers have zero angular momentum with respect to infinity. Of course, since the rotation of geometry imposes frame dragging, the observer will always have non-zero angular velocity with respect to infinity near the horizon r_+. These observer posses an important geometrical property: they are orthogonal to hypersurfaces of constant t [9].

Consider an observer with the four velocity

$$\mathbf{u} = u^t(\boldsymbol{\partial}_t + \tilde{\omega}\boldsymbol{\partial}_\varphi), \tag{2.9}$$

with u^t being the normalization factor such that $u^\mu u_\mu = -1$. The angular momentum per unit mass of such observer is

$$\tilde{L} \equiv u_\varphi = g_{\varphi\varphi} u^t \left(\tilde{\omega} - \frac{2Mar}{A}\right), \tag{2.10}$$

where $A = \Sigma\Delta + 2Mr(r^2 + a^2)$. The ZAMO observer are characterizes by $\tilde{\omega} = \omega \equiv \frac{2Mar}{A}$, then $u^t = \sqrt{\frac{A}{\Sigma\Delta}}$. The whole tetrad is then given by

$$\begin{aligned}
\mathbf{e}_{(t)} &= u^t(\boldsymbol{\partial}_t + \omega\boldsymbol{\partial}_\varphi), \\
\mathbf{e}_{(r)} &= \sqrt{\frac{\Delta}{\Sigma}}\boldsymbol{\partial}_r, \\
\mathbf{e}_{(\theta)} &= \Sigma^{-1/2}\boldsymbol{\partial}_\theta, \\
\mathbf{e}_{(\varphi)} &= \sqrt{\frac{\Sigma}{A}}\frac{1}{\sin\theta}\boldsymbol{\partial}_\varphi.
\end{aligned} \tag{2.11}$$

Such observer move with $\varphi = \omega t + const$ and stay at $r = const., \theta = const.$ and have a clear meaning anywhere above the outer horizon r_+

By radially boosting the ZAMO observer it is possible to create a family of free falling observers. These observers still have zero angular momentum and fall along the coordinate lines $\theta = const.$ The whole tetrad is given in [10].

Doran tetrad

The ZAMO tetrad has no physical meaning on the horizon $r = r_+$. For inquires about near horizon behaviour and even behaviour under the horizon it is more appropriate to choose some more well defined tetrad. One of such is the Doran tetrad [5]. Which is natural to the Doran coordinates (1.14).

The tetrad represents observers who are freely falling along radial trajectories, starting at rest at radial infinity while maintaining $\tilde{\varphi} = const, \theta = const.$. This tetrad has the four-velocity

$$\tilde{\mathbf{u}} = -\mathbf{d}\tilde{t}. \tag{2.12}$$

It holds that

$$\tilde{u}^a \nabla_a \tilde{u}^b = 0, \tag{2.13}$$

so the Doran observers really do form a congruence of free falling timelike observers. Such motion is almost Newtonian and the proper time of the observer coincides with the coordinate time $\tilde{t}$. The whole tetrad in the Boyer-Lindquist coordinates takes the form

$$\tilde{\mathbf{u}} = \tilde{\mathbf{e}}_{(t)} = -\mathbf{d}t - \frac{\sqrt{2Mr(r^2 + a^2)}}{\Delta}\mathbf{d}r,$$

$$\tilde{\mathbf{e}}_{(r)} = \sqrt{\frac{2Mr}{\Sigma}}(\mathbf{d}r - a\sin^2\theta \mathbf{d}\varphi) + \frac{\sqrt{\Sigma(r^2 + a^2)}}{\Delta}\mathbf{d}r,$$

$$\tilde{\mathbf{e}}_{(\theta)} = \sqrt{\Sigma}\mathbf{d}\theta, \tag{2.14}$$

$$\tilde{\mathbf{e}}_{(\varphi)} = \frac{\sqrt{2Mr}a\sin\theta}{\Delta}\mathbf{d}r + \sqrt{r^2 + a^2}\sin\theta \mathbf{d}\varphi.$$

2.2 Newman-Penrose Formalism

Newman-Penrose formalism [11] is a special case of tetrad formalism, where we choose two real vectors and a complex-conjugate pair denoted $\mathbf{l}$, $\mathbf{n},\mathbf{m}$ and $\overline{\mathbf{m}}$. Which satisfy

$$l^a l_a = n^a n_a = m^a m_a = \overline{m}^a \overline{m}_a = l^a m_a = n^a m_a = l^a \overline{m}_a = n^a \overline{m}_a = 0, \tag{2.15}$$

and

$$l^a n_a = -m^a \overline{m}_a = 1. \tag{2.16}$$

Under these conditions the metric tensor can be expressed as

$$g_{ab} = -l_a n_b - l_b n_a + m_a \overline{m}_b + m_b \overline{m}_a. \tag{2.17}$$

The basis is identified as

$$\mathbf{e}_1 = \mathbf{l}, \quad \mathbf{e}_2 = \mathbf{n}, \quad \mathbf{e}_3 = \mathbf{m}, \quad \mathbf{e}_4 = \overline{\mathbf{m}}. \tag{2.18}$$

It is also customary to define special symbols for the diractional derivatives

$$D \equiv l^a \frac{\partial}{\partial x^a}, \quad \Delta \equiv n^a \frac{\partial}{\partial x^a} \quad \delta \equiv m^a \frac{\partial}{\partial x^a}, \quad \overline{\delta} \equiv \overline{m}^a \frac{\partial}{\partial x^a}. \tag{2.19}$$

If the (2.16) equations are to be satisfied the matrix $\eta_{(a)(b)}$ must take form

$$\eta_{(a)(b)} = \begin{pmatrix} 0 & 1 & 0 & 0 \\ 1 & 0 & 0 & 0 \\ 0 & 0 & 0 & -1 \\ 0 & 0 & -1 & 0 \end{pmatrix}. \tag{2.20}$$

Usually twelve special symbols are defined for Ricci rotation coefficients

$$\begin{aligned}
\kappa &= \gamma_{(3)(1)(1)}, \quad \sigma = \gamma_{(3)(1)(3)}, \quad \lambda = \gamma_{(2)(4)(4)}, \quad \nu = \gamma_{(2)(4)(2)}, \\
\rho &= \gamma_{(3)(1)(4)} \quad \mu = \gamma_{(2)(4)(3)}, \quad \tau = \gamma_{(3)(1)(2)}, \quad \pi = \gamma_{(2)(4)(3)}, \\
\epsilon &= \frac{1}{2}(\gamma_{(2)(1)(1)} + \gamma_{(3)(4)(1)}), \quad \gamma = \frac{1}{2}(\gamma_{(2)(1)(2)} + \gamma_{(3)(4)(2)}), \\
\alpha &= \frac{1}{2}(\gamma_{(2)(1)(4)} + \gamma_{(3)(4)(4)}), \quad \beta = \frac{1}{2}(\gamma_{(2)(1)(3)} + \gamma_{(3)(4)(3)}).
\end{aligned} \tag{2.21}$$

Finally the so called *intrinsic derivative* is also defined

$$A_{(a)|(b)} = A_{(a);(b)} - \eta^{(n)(m)}\gamma_{(n)(a)(b)}A_{(m)}. \tag{2.22}$$

As we can see from the Einstein equations (1.1), the Riemann curvature tensor is of prime importance in GR, the tensor describes the non-commutativity of differentiation when applied to a dual vector field. The Ricci tensor, a derived quantity from the Riemann tensor, describes the deformation of such an object. Finally the Weyl tensor, which measures the tidal forces on an object moving along geodesics, is defined as a trace-free part of Riemann tensor, i.e.

$$C_{abcd} = R_{abcd} - g_{a[a}R_{d]b} - \frac{1}{3}R g_{a[c}g_{d]b}, \tag{2.23}$$

where R is scalar curvature and $R_{ab} = R_{abc}{}^{b}$ is the Ricci tensor.

Projecting the Weyl tensor into tetrad basis we get [8].

$$C_{(a)(b)(c)(d)} = R_{(a)(b)(c)(d)} - \eta_{(a)[(a)}R_{(d)](b)} - \frac{1}{3}R\eta_{(a)[(c)}\eta_{(d)](b)}, \tag{2.24}$$

with $R_{(a)(b)}$ denoting the tetrad components of Ricci tensor and R the tetrad components of the scalar curvature

$$R_{(a)(c)} = \eta^{(b)(d)}R_{(a)(b)(c)(d)}, \quad R = \eta^{(a)(b)}R_{(a)(b)}. \tag{2.25}$$

In NP formalism Weyl tensor is represented by 5 complex scalars

$$\begin{aligned}
\psi_0 &= -C_{(1)(3)(1)(3)}, \\
\psi_1 &= -C_{(1)(2)(1)(3)}, \\
\psi_2 &= -C_{(1)(3)(4)(2)}, \\
\psi_3 &= -C_{(1)(2)(4)(2)}, \\
\psi_4 &= -C_{(2)(4)(2)(4)},
\end{aligned} \tag{2.26}$$

and the 10 independent components of Ricci tensor are represented by four real scalars $(\Phi_{00}, \Phi_{11}, \Phi_{22}, \Lambda)$ and three complex ones $\Psi_{10}, \Psi_{20}, \Psi_{21}$ along with their complex conjugates.

$$\begin{aligned}
\Psi_{00} &= \frac{1}{2}R_{(1)(1)}, \quad \Psi_{11} = \frac{1}{4}(R_{(1)(2)} - R_{(3)(4)}), \quad \Psi_{22} = \frac{1}{2}R_{(2)(2)}, \\
\Lambda &= \frac{R}{24}, \quad \Psi_{10} = \frac{1}{2}R_{(1)(4)}, \quad \Psi_{20} = \frac{1}{2}R_{(4)(4)}, \quad \Psi_{21} = \frac{1}{2}R_{(4)(3)}.
\end{aligned} \tag{2.27}$$

2.2.1 Petrov classification

In the NP formalism we can elegantly formulate the Petrov classification scheme of the Weyl tensor, which describes possible algebraic symmetries of the tensor [4]. For non-conformally flat spacetime ($C_{abcd} \neq 0$) we usually classify spacetimes by the Petrov-Penrose classification of the Weyl tensor. Consider the transformation (so called null rotation about $\mathbf{n}$)

$$\mathbf{n}' = \mathbf{n}, \ \mathbf{m}' = \mathbf{m} + b\mathbf{n}, \ \mathbf{l}' = \mathbf{l} + b^*\mathbf{m} + b\overline{\mathbf{m}} + bb^*\mathbf{n} \tag{2.28}$$

where b is a complex parameter, let us quickly note that multiple classes of transformation of type (2.28) exist, for example Griffiths and Podolský [4] classify the Weyl tensor by null rotations about $\mathbf{l}$ (class I), here we follow Chandrasekhar [8] who classifies the Weyl tensor under the transformation (2.28) (class II). Under this transformation the Weyl scalars (2.26) transform as

$$\begin{aligned}
\Psi_0' &= \Psi_0 + 4b\Psi_1 + 6b^2\Psi_2 + 4b^3\Psi_3 + b^4\Psi_4, \\
\Psi_1' &= \Psi_1 + 3b\Psi_2 + 3b^2\Psi_3 + b^3\Psi_4, \\
\Psi_2' &= \Psi_2 + 2b\Psi_3 + b^2\Psi_4, \\
\Psi_4' &= \Psi_4.
\end{aligned}$$

We can immediately see that

$$\Psi_0' = 0 \iff \Psi_0 + 4b\Psi_1 + 6b^2\Psi_2 + 4b^3\Psi_3 + b^4 = 0. \tag{2.29}$$

This quartic equation has four roots from which we can recover new $\mathbf{l}$, which we call the *principal directions* of Weyl tensor. Depending on the roots we classify the spacetimes as

> type I : four distinct roots
> type II : two identical roots, two distinct
> type D : two pairs of identical roots
> type III : three identical, one distinct
> type N : four identical roots

In *type D* spacetimes the we can have such a tetrad that
$\Psi_0 = \Psi_1 = \Psi_4 = \Psi_3 = 0, \Psi_2 \neq 0$ and $\kappa = \sigma = \nu = \lambda = 0$ - this is content of Golber-Sachs theorem [12].

We will later, by explicit calculation show, that the Kerr metric is of the Type D. This will allow us to utilize special relation which hold in this type of spacetime to completely solve the Maxwell equation for a given test field source.

2.2.2 Maxwell Equations in NP Formalism

For our purposes, Maxwell equations are most important. As with any tensor, the EM tensor can be projected onto the null tetrad; since the EM tensor is antisymmetric we get three complex scalars

$$\begin{aligned}
\phi_0 &= F_{ij}l^i m^j, \\
\phi_1 &= \frac{1}{2}F_{ij}(l^i n^j + \overline{m}^j m^j), \\
\phi_2 &= F_{ij}\overline{m}^i n^j.
\end{aligned} \tag{2.30}$$

From these NP scalar we can reconstruct the Maxwell tensor as follows

$$F_{ij} = 2 \left[\phi_1 \left(n_{[i}l_{j]} + m_{[i}\overline{m}_{j]} \right) + \phi_0 \, l_{[i}m_{j]} + \phi_2 \, \overline{m}_{[i}n_{j]} \right] + c.c. \qquad (2.31)$$

Where square brackets over indices indicate antisymetrization and *c.c* is complex conjugate.

The source free Maxwell equations are

$$F_{[ij;k]} = 0, \quad g^{ij} F_{ik,j} = 0 \qquad (2.32)$$

these take the form

$$\begin{aligned}
\phi_{1|(1)} - \phi_{0|(4)} &= 0, \quad \phi_{2|(1)} - \phi_{1|(4)} = 0, \\
\phi_{1|(3)} - \phi_{0|(2)} &= 0, \quad \phi_{2|(3)} - \phi_{1|(2)} = 0.
\end{aligned} \qquad (2.33)$$

The source-free Maxwell equations with zero four-current (3.3) can be written explicitly in terms of directional derivatives and Ricci rotations coefficients as

$$\begin{aligned}
D\phi_1 - \overline{\delta}\phi_0 &= (\kappa - 2\alpha)\phi_0 + 2\rho\phi_1 - \kappa\phi_2, \\
D\phi_2 - \overline{\delta}\phi_1 &= -\lambda\phi_0 + 2\pi\phi_1 + (\rho - 2\epsilon)\phi_2, \\
\delta\phi_1 - \Delta\phi_0 &= (\mu - 2\gamma)\phi_0 + 2\tau\phi_1 - \sigma\phi_2, \\
\delta\phi_2 - \Delta\phi_1 &= -\nu\phi_0 + 2\mu\phi_1 + (\tau - 2\beta)\phi_2.
\end{aligned} \qquad (2.34)$$

We want to quickly note that the NP formalism in neatly implemented (although with missing documentation) in the Mathematica package xAct [13]. We've used this package for nearly all tensorial and NP calculations

3. Maxwell equations

Although we have already formulated the Maxwell equations in the so called NP formalism. We still want to give a short review of Maxwell equations in the more traditional tensorial formalism. A more exhaustive introduction to electromagnetic theory can be found in [14]. From this we will be able to discuss the invariants of the Maxwell field which are, as any invariant in GR, of prime importance.

On a general four dimensional manifold M the Maxwell equations can be formulated as

$$\begin{aligned} \mathrm{d}\mathbf{F} &= 0 \\ \mathrm{d} \star \mathbf{F} &= \mathbf{J} \end{aligned} \tag{3.1}$$

Where $\mathbf{F} = \mathrm{d}\mathbf{A}$ is the Maxwell tensor, d is the exterior derivative and $\mathbf{J}$ is the current 3-form which satisfies the continuity equation

$$\mathrm{d}\mathbf{J} = 0 \tag{3.2}$$

In a coordinates basis $\partial_x{}^\mu$ the equations (3.1) (3.2) are

$$\begin{aligned} F^{[\alpha\beta;\gamma]} &= 0, \\ F^{\alpha\beta}{}_{;\beta} &= 4\pi J^\alpha. \end{aligned} \tag{3.3}$$

The electric field $\mathbf{E}$ and magnetic field $\mathbf{B}$ can be identified by defining an appropriate observer four-velocity $\mathbf{u}$ and projecting the Maxwell tensor $\mathbf{F}$ onto this four-velocity.

$$\begin{aligned} B^\mu &= -\frac{1}{2}\epsilon^{\mu\nu\sigma\rho}u_\nu F_{\sigma\rho}, \\ E^\mu &= F^{\mu\nu}u_\nu. \end{aligned} \tag{3.4}$$

As we can see the equations are of course, in adherence to the principle of general covariance, covariant. However it is important to remember that, although the Maxwell tensor $\mathbf{F}$ is a physical quantity, we usually discuss the components in relation to a specified coordinates. Thus the components can change depending on the coordinates we choose. It's often useful to find some truly invariant quantities — scalars. These can be easily constructed from the Maxwell tensor.

$$\begin{aligned} \frac{1}{2}F^{\alpha\beta}F_{\alpha\beta} &= B^\alpha B_\alpha - E^\alpha E_\alpha = ||\mathbf{B}||^2 - ||\mathbf{E}||^2 \\ \left(\frac{1}{4}F^{\alpha\beta} \star F_{\alpha\beta}\right)^2 &= (B^a E_a)^2 = (\mathbf{B} \cdot \mathbf{E})^2 \end{aligned} \tag{3.5}$$

The square in the latter equation was taken to construct a true scalar. Otherwise the expression $\mathbf{B}\cdot\mathbf{E}$ is a pseudoscalar since $\mathbf{E}$ is a tensor and $\mathbf{B}$ is an pseudotensor, this can be seen at first glance since there is the Levi-Civita tensor in the definition of the magnetic field.

We can understand these two scalars as follows. The latter of (3.5) states that if the electric and magnetic field are perpendicular in any reference system,

then they are perpendicular in all systems and that we can always find a reference system in which $\mathbf{E} = 0$ or $\mathbf{B} = 0$. The former clearly related that the comparative magnitudes stays the same in all reference systems. Since the two invariants (3.5) are fundamental, any other invariant of the electromagnetic field can be constructed from these two. We will now illustrate by calculating other possible invariants.

First we define the self-dual form.

$$^*\mathbf{F} = \mathbf{F} - i \star \mathbf{F} \tag{3.6}$$

where $\star$ is the Hodge dual. Such form is convenient since it allows us to encode the electric and magnetic field into a single complex vector. Consider some observer four-velocity $\mathbf{u} \cdot \mathbf{u} = -1$ we then get

$$^*F^{ab}u_b = E^a + iB^a \tag{3.7}$$

We can now encode the invariant into a single complex scalar

$$\frac{1}{4} {}^*F^{ab*}F_{ab} = \frac{1}{2}(F^{ab}F_{ab} + iF^{ab} \star F_{ab}) = 2iB^a E_a + B^a B_a - E^a E_a \tag{3.8}$$

If the scalar above is zero we say that the electromagnetic field is null [4] which is equivalent to formulation above that the electric and magnetic fields are orthogonal, have equal magnitude and propagate at the speed of light.

When analytic results are not available, we use numeric results usually accompanied with graphic visualization. For this real invariants are preferred, we can make the invariant (3.8) real by taking the hermitian conjugate

$$\frac{1}{16} {}^*F^{ab*}F_{ab}\overline{{}^*F}^{cd}\overline{{}^*F}_{cd} = (||\mathbf{B}||^2 - ||\mathbf{E}||^2)^2 + 4(\mathbf{B} \cdot \mathbf{E})^2, \tag{3.9}$$

Even thought the scalar above is real, it should be noted that it still holds that the field is null only if the scalar $^*F^{ab*}F_{ab}\overline{{}^*F}^{cd}\overline{{}^*F}_{cd}$ is zero, since it's split into two non-negative parts. To infer the meaning of the scalar (3.9) we will now express some identities in the NP basis, we can do this since all basis are equally good for invariants.

Consider the energy momentum tensor (1.3) $T^a{}_b$, expressing this in the NP basis (2.18) and (2.31) we get

$$T^{(a)}{}_{(b)} = 2 \begin{pmatrix} -\overline{\phi_1}\phi_1 & -\overline{\phi_2}\phi_2 & -\overline{\phi_2}\phi_1 & -\overline{\phi_1}\phi_2 \\ -\overline{\phi_0}\phi_0 & -\overline{\phi_1}\phi_1 & -\overline{\phi_1}\phi_0 & -\overline{\phi_0}\phi_1 \\ \overline{\phi_0}\phi_1 & \overline{\phi_1}\phi_2 & \overline{\phi_1}\phi_1 & \overline{\phi_0}\phi_2 \\ \overline{\phi_1}\phi_0 & \overline{\phi_2}\phi_1 & \overline{\phi_2}\phi_0 & \overline{\phi_1}\phi_1 \end{pmatrix}. \tag{3.10}$$

Computing the eigenvalues of this we get

$$\lambda_1 = \lambda_2 = -\lambda_3 = -\lambda_4 = 2\sqrt{(\phi_1^2 - \phi_0\phi_2)(\overline{\phi}_1^2 - \overline{\phi}_0\overline{\phi}_2)} \ . \tag{3.11}$$

Since the eigenvalue equation $\mathbf{Tv} = \lambda\mathbf{v}$ is basis invariant, the scalar λ_i is an invariant quantity, this can be seen by expressing it terms of the two invariants of the electromagnetic field. Expressing the invariant (3.9) in the NP basis we get

$$^*F^{ab*}F_{ab}\overline{{}^*F}^{cd}\overline{{}^*F}_{cd} = 256(\phi_1^2 - \phi_0\phi_2)(\overline{\phi}_1^2 - \overline{\phi}_0\overline{\phi}_2) \tag{3.12}$$

Working out the factors we get

$$\frac{1}{8}\sqrt{{}^*F^{ab}{}^*F_{ab}\overline{{}^*F^{cd}{}^*F_{cd}}} = \lambda_1 = -\lambda_3 \tag{3.13}$$

Thus we get that the invariant (3.9) is in fact the square of the eigenvalue of the energy momentum tensor of the Maxwell field. Let us now define the Poynting vector as

$$P^a = -T^{ab}u_b \tag{3.14}$$

expressing the Poynting vector in terms of the electric **E** and magnetic **B** fields

$$P^a = \frac{1}{2}u^a(B_bB^b + E_bE^b) + \epsilon^a{}_{bcd}u^bB^cE^d \tag{3.15}$$

this definition recovers the standard three vector Poyting in the tetrad indices

$$P_{(a)} = \epsilon_{(a)(b)(c)}B^{(c)}E^{(b)}, \quad a = 1, 2, 3, \tag{3.16}$$

with and the zero element is

$$P^{(0)} = \frac{1}{2}(||\mathbf{E}||^2 + ||\mathbf{B}||^2). \tag{3.17}$$

calculating the norm of the Poyting vector we get the relation

$$P^aP_a = T_{ab}T^{ac}u^bu_c = \lambda_1 = -\lambda_3 \tag{3.18}$$

Thus the invariant takes a clear meaning, it is simply the square root of the norm of the Poyting four-vector and as is clear from the eigenvalues (3.11) this is independent of the choice of four-velocity **u**.

4. Solving the Maxwell equations

We will start from Teukolsky's article [15], in which he, among others, derives linearized equations for gravitational and electromagnetic fields of a rotating black hole. It turns out that the standard calculation procedure, in which the metric perturbation is taken into account, gives too complex results and inseparable equations. Teukolsky therefore uses the NP formalism - for each NP quantity and for each NP tetrad vector X, it holds that $X = X_A + X_B$, where X_A is the quantity corresponding to the background and X_B its perturbation. By substituting into the NP equations and leaving only the terms linear in B, we obtain the desired equations.

First we have to choose an appropriate tetrad. For the sake of consistency with other related works we choose the so called Kinnersley tetrad. Such tetrad is appropriate due to the fact that many of the Ricci spin coefficients $\kappa, \sigma, \nu, \lambda, \epsilon$ are zero and all but one of projections of Weyl tensor are zero.

$$
\begin{aligned}
\mathbf{l} &= \frac{1}{\Delta}\left[\left(r^2 + a^2\right)\boldsymbol{\partial}_t + \Delta\boldsymbol{\partial}_r + a\boldsymbol{\partial}_\varphi\right], \\
\mathbf{n} &= \frac{1}{2\Sigma}\left[\left(r^2 + a^2\right)\boldsymbol{\partial}_t - \Delta\boldsymbol{\partial}_r + a\boldsymbol{\partial}_\varphi\right], \\
\mathbf{m} &= \frac{1}{\sqrt{2}\overline{\varrho}}\left[ia\sin\theta\boldsymbol{\partial}_t + \boldsymbol{\partial}_\theta + \frac{i}{\sin\theta}\boldsymbol{\partial}_\varphi\right].
\end{aligned}
\tag{4.1}
$$

The full Ricci rotation coefficients (2.21) then read

$$
\begin{aligned}
&\mu = \tfrac{1}{2}\Delta\rho^2\bar{\rho}, &&\tau = -\tfrac{i}{\sqrt{2}}a\sin\theta\rho\bar{\rho}, \\
&\pi = \tfrac{i}{\sqrt{2}}a\sin\theta\rho^2, &&\gamma = \mu + \tfrac{1}{2}(-M + r)\rho\bar{\rho}, \\
&\alpha = -\bar{\beta} + \pi, &&\beta = -\tfrac{1}{2\sqrt{2}}\cot\theta\bar{\rho}, \\
&\rho = \frac{1}{\varrho} = \frac{1}{ia\cos\theta - r}, &&\kappa = \sigma = \alpha = \nu = \epsilon = 0.
\end{aligned}
\tag{4.2}
$$

Where we also defined ϱ. Since we are in Type D spacetime with an appropriate tetrad the only non-zero Weyl scalar is

$$
\Psi_2 = -\frac{M}{\varrho^3}.
\tag{4.3}
$$

4.1   Electromagnetism in Type D spacetime

Omitting the index $_B$, the linearized equations for the perturbed electromagnetic field are

$$
(D - 2\rho)\phi_1 - (\bar{\delta} + \pi - 2\alpha)\phi_0 = 2\pi J_l,
\tag{4.4}
$$

$$
(\delta - 2\tau)\phi_1 - (\Delta + \mu - 2\gamma)\phi_0 = 2\pi J_m,
\tag{4.5}
$$

$$
(D - \rho + 2\epsilon)\phi_2 - (\bar{\delta} + 2\pi)\phi_1 = 2\pi J_{\overline{m}},
\tag{4.6}
$$

$$
(\delta - \tau + 2\beta)\phi_2 - (\Delta + 2\mu)\phi_1 = 2\pi J_n.
\tag{4.7}
$$

The lower index next to J denotes the projection of the four vector $J^\mu + iM^\mu$, where we also included the magnetic current vector M^μ onto the NP tetrad components. For example $J_l = (J^\mu + iM^\mu)l_\mu$.

Utilising the following commutation relation, which hold for any Type D metric [2],

$$(D - \epsilon + \bar{\epsilon} - 2\rho - \bar{\rho})(\delta - 2\tau) - (\delta - \beta - \bar{\alpha} + \bar{\pi} - 2\tau)(D - 2\rho) = 0, \qquad (4.8)$$

and applying $(\delta - \beta - \bar{\alpha} + \bar{\pi} - 2\tau)$ on (4.4) and $(D - \epsilon + \bar{\epsilon} - 2\rho - \bar{\rho})$ on (4.5) we get by the difference of these equations

$$\begin{aligned}
\left[(D - \epsilon + \bar{\epsilon} + 2\mu + \bar{\mu})(\Delta + \mu - 2\gamma)\right. & \\
\left. + (-\delta + \beta + \bar{\alpha} + 2\tau - \bar{\pi})(\bar{\delta} + \pi - 2\alpha)\right] \phi_0 &= 2\pi J_0,
\end{aligned} \qquad (4.9)$$

with

$$J_0 = (\delta - \beta - \bar{\alpha} - 2\tau + \bar{\pi})J_l - (D - \epsilon + \bar{\epsilon} - 2\rho - \bar{\rho})J_m.$$

Under the interchange of $\mathbf{l}$ with $\mathbf{n}$ and $\mathbf{m}$ with $\bar{\mathbf{m}}$ we get

$$\begin{aligned}
\left[(\Delta + \gamma - \bar{\gamma} + 2\mu + \bar{\mu})(D - \rho + 2\epsilon)\right. & \\
\left. - (\bar{\delta} + \alpha + \bar{\beta} + 2\pi - \bar{\tau})(\delta - \tau + 2\beta)\right] \phi_2 &= 2\pi J_2,
\end{aligned} \qquad (4.10)$$

with

$$J_2 = (\Delta + \gamma - \bar{\gamma} + 2\mu + \bar{\mu})J_{\bar{m}} - (\bar{\delta} + \alpha + \bar{\beta} + 2\pi - \bar{\tau})J_n. \qquad (4.11)$$

Astoundingly, not only equations (4.9) and (4.10), but also the equations for gravitational field and neutrino field can be summarised in the so-called Teukolsky's master equation [15]. In Boyer-Lindquist coordinates with the (4.1) it reads

$$\begin{aligned}
&\left(\frac{(r^2 + a^2)^2}{\Delta} - a^2 \sin^2\theta\right)\frac{\partial^2\psi}{\partial t^2} + \frac{4Mar}{\Delta}\frac{\partial^2\psi}{\partial t\partial\varphi} + \left(\frac{a^2}{\Delta} - \frac{1}{\sin^2\theta}\right)\frac{\partial^2\psi}{\partial\varphi^2} \\
&- \Delta^{-s}\frac{\partial}{\partial r}(\Delta^{s+1}\frac{\partial\psi}{\partial r}) - \frac{1}{\sin\theta}\frac{\partial}{\partial\theta}(\sin\theta\frac{\partial\psi}{\partial\theta}) - 2s\left(\frac{a(r - M)}{\Delta} + \frac{i\cos\theta}{sin^2\theta}\right)\frac{\partial\psi}{\partial\varphi} \\
&- 2s\left(\frac{M(r^2 - a^2)}{\Delta} - \bar{\varrho}\right)\frac{\partial\psi}{\partial t} + (s^2 + \cot^2\theta - s)\psi = 4\pi\Sigma T.
\end{aligned}$$
$$(4.12)$$

For electromagnetic perturbations we recover our fore-mentioned (4.9) (4.10) by plugin in $\{\psi = \phi_0, s = 1, T = J_0\}$ or $\{\psi = \rho^{-2}\phi_2, s = -1, T = \rho^{-2}J_2\}$ respectively. Furthermore Bičák, Janiš [2] showed that these equations are separable for stationary solutions by utilising the ansatz.

$$\begin{aligned}
\phi_1 &= \left(\frac{r_+ - r_-}{\varrho}\right)^2 \sum_{l,m} {}^0R_{lm}\,{}_1Y_{lm}(\theta, \varphi), \\
\phi_2 &= \left(\frac{r_+ - r_-}{\varrho}\right)^2 \sum_{l,m} {}^2R_{lm}(r)\,{}_{-1}Y_{lm}(\theta, \varphi).
\end{aligned} \qquad (4.13)$$

Where $\sum_{l,m}$ abbreviates $\sum_{l=1}^{\infty}\sum_{m=-l}^{l}$, Y_{lm} are the NP spin-weighted spherical harmonics (see appendix A.1). The factors before the sum have been introduced

in [2] to further simplify the equations. Utilising the orthonormality of the spin-weighted spherical harmonics and the equations for ϕ_2 we obtain [2]

$$\Delta\frac{d^2({}^2R_{lm})}{dr^2} + \left[\frac{a^2m^2 - 2iam(r-M)}{\Delta} - l(l+1)\right]{}^2R_{lm} = -4\pi^2 J_{lm}. \qquad (4.14)$$

Where

$$^2J_{lm} = \int_0^{2\pi}\int_0^\pi d\theta d\varphi \frac{\Sigma \,\varrho^2\, J_2}{(r_+ - r_-)^2}\, {}_{-1}\overline{Y}_{lm}\sin\theta, \qquad (4.15)$$

$$J_2 = \frac{-\Delta}{2\sqrt{2}\Sigma\varrho^2}\Bigl[\sqrt{2}\left(\frac{\partial}{\partial r} - \frac{a}{\Delta}\frac{\partial}{\partial\varphi} + \frac{1}{\varrho}\right)\varrho^2 J_{\overline{m}}$$
$$+ 2\left(\frac{\partial}{\partial\theta} - \frac{i}{\sin\theta}\frac{\partial}{\partial\varphi} + \frac{ia\sin\theta}{\varrho}\right)\frac{\Sigma\varrho}{\Delta}J_n\Bigr]. \qquad (4.16)$$

We could have derived similar equations for φ_0. But in [2] a relation has been found between ${}^0R_{lm}$ and ${}^2R_{lm}$, by applying differential operators to the Maxwell equations we get

$$^0R_{lm} = \frac{2(r_+ - r_-)^2}{l(l+1)}\left(\frac{d}{dr} + \frac{iam}{\Delta}\right)\left(\frac{d}{dr} + \frac{iam}{\Delta}\right){}^2R_{lm}. \qquad (4.17)$$

Since no separated equation for ϕ_1 exists. We can utilize the normal Maxwell equations. Thanks to axial symmetry we write

$$\phi_1(x,\theta,\phi) = \sum_{m=-\infty}^{\infty}\left(1 - \frac{1}{x}\right)^{\frac{-iam}{r_+ - r_-}} e^{im\phi}\phi_{lm}(x,\theta). \qquad (4.18)$$

Using this ansatz, [2] we are able to express ϕ_1 as function of ${}^2y_{lm}$.

The homogeneous part of the equation (4.14) is of the Fuchsian type. The equation has three regular singular points $\{r_-, r_+, \infty\}$. We can transform such equation into a hypergeometric form. For our equation the transformation reads

$$^2R_{lm}(x) = \left(1 - \frac{1}{x}\right)^{iZ_m}{}^2y_{lm}(x),$$
$$x = \frac{r - r_-}{r_+ - r_-} \quad Z_m = \frac{am}{r_+ - r_-}, \qquad (4.19)$$

we get

$$x(x-1)\,{}^2y_{lm}'' - 2iZ_m\,{}^2y_{lm}' - l(l+1){}^2y_{lm} = 0. \qquad (4.20)$$

The two solutions are

$$^2y_{lm}^I = \left(1 - \frac{1}{x}\right)^{2iZ_m} x(x-1)\,{}_2F_1(l+1, 1-l, 2-2iZ_m, x),$$
$$^2y_{lm}^{II} = (-x)^{-l}\,{}_2F_1(l, l+1-2iZ_m, 2l+2, x), \qquad (4.21)$$

where ${}_2F_1$ denotes the hypergeometric function of the second type [16]. The solution I corresponds to the inner solution $r < r_0$ where r_0 is the location of the source. The solution II corresponds to the outer solution $r_0 < r$. These solutions were chosen such that the functions ${}^0R_{lm}^I$ and ${}^2R_{lm}^I$ are admissible at the horizon

r_+ and such that $^0R_{lm}^{II}$ and $^2R_{lm}^{II}$ are admissible at infinity. Finally the complete inner solution is

$$\phi_0 = \sum_{l,m} \frac{2\,a_{lm}}{l(l+1)}\left(1 - \frac{1}{x}\right)^{-iZ_m} \frac{d^2}{dx^2}\left(^2y_{lm}^I\right)\,_1Y_{lm},$$

$$\phi_1 = \frac{E_a}{\varrho^2} + \frac{\sqrt{2}\,(r_+ - r_-)}{\varrho^2} \sum_{l,m} \frac{a_{lm}}{l(l+1)}\left(1 - \frac{1}{x}\right)^{-iZ_m}\left\{-ia\sin\theta\frac{d}{dx}\left(^2y_{lm}^I\right)\,_1Y_{lm}\right.$$

$$\left. + [l(l+1)]^{1/2}\left[\varrho\,\frac{d}{dx}\left(^2y_{lm}^I\right) - (r_+ - r_-)\,^2y_{lm}^I\right]\,_0Y_{lm}\right\},$$

$$\phi_2 = \frac{(r_+ - r_-)^2}{\varrho^2} \sum_{l,m} \alpha_{lm}\left(1 - \frac{1}{x}\right)^{-iZ_m}\,_2y_{lm}^I\,_{-1}Y_{lm}.$$

(4.22)

For the outer solution we can just replace α_{lm} with β_{lm} and $^2y_{lm}^I$ with $^2y_{lm}^{II}$. To determine α_{lm} and β_{lm} we take the full solution of inhomogeneous equation (4.14)

$$^2R_{lm}(x) = {}^2R_{lm}^I(x)\int \frac{4\pi^2 J_{lm}(\xi)^2 R_{lm}^{II}(\xi)}{\xi(\xi - 1)W(^2R_{lm}^{II},\,^2R_{lm}^I,\xi)}\mathrm{d}\xi$$

$$- {}^2R_{lm}^{II}(x)\int \frac{4\pi^2 J_{lm}(\xi)^2 R_{lm}^{II}(\xi)}{\xi(\xi - 1)W(^2R_{lm}^{II},\,^2R_{lm}^I,\xi)}\mathrm{d}\xi,$$

(4.23)

where

$$W(^2R_{lm}^{II},\,^2R_{lm}^I,\xi) = \frac{(2l+1)!\Gamma(2 - 2iZ_m)}{(l+1)!\Gamma(l+1 - 2iZ_m)},$$

(4.24)

is the Wronskian at the points ξ. Comparing (4.23) with (4.45) while regarding the substitution (4.19) and solution (4.21) we get

$$\alpha_{lm} = -4\pi\,W(^2R_{lm}^{II},\,^2R_{lm}^I,\xi)\int \frac{^2J_{lm}(\xi)\,^2R_{lm}^{II}(\xi)}{\xi(\xi - 1)}\mathrm{d}\xi,$$

$$\beta_{lm} = -4\pi\,W(^2R_{lm}^{II},\,^2R_{lm}^I,\xi)\int \frac{^2J_{lm}(\xi)\,^2R_{lm}^I(\xi)}{\xi(\xi - 1)}\mathrm{d}\xi.$$

(4.25)

Lastly, we need to determine the constants E_a and E_b. To do this we employ the Gauss theorem, which can be written as

$$\int_0^{2\pi}\int_0^{\pi}(-g)^{1/2}F^{tr}|_{r=r_0}\mathrm{d}\theta\mathrm{d}\varphi = 4\pi e(r_0),$$

(4.26)

where r_0 is the total charge inside the "sphere" of radius r_0. Expressing out the F^{tr} explicitly

$$F_{r=r_0}^{tr} = \left\{\frac{(r^2 + a^2)}{\Sigma}\phi_1 - \frac{ia\sin\theta}{\sqrt{2}\overline{\varrho}}\phi_2 + \frac{ia\Delta\sin\theta}{2\sqrt{2}\Sigma\varrho}\phi_0 + \text{c.c.}\right\}|_{r=r_0}.$$

(4.27)

Where c.c. denotes the complex conjugate. Only the axisymmetric terms ($m = 0$) contribute to the integral (4.26) owing to the integration over φ. Keeping this in

mind we only need to evaluate

$$
\int_{-1}^{1} \left[\frac{\sqrt{l(l+1)}\,_0Y_{l0}(\theta,0)}{r_0 - ia\cos\theta} - \frac{ia\sin\theta\,_1Y_{l0}(\theta,0)}{(r_0 - ia\cos\theta)^2} \right] \mathrm{d}(\cos\theta) =
$$

$$
= \int_0^{\pi} \left[\frac{\frac{i}{\sin\theta}\frac{\partial}{\partial\theta}\left(\sin\theta\,_1Y_{l0}(\theta,0)\right)}{r_0 - ia\cos\theta} + \frac{\partial}{\partial\theta}\left(r_0 - ia\cos\theta\right)^{-1}\,_1Y_{l0}(\theta,0) \right] \sin\theta\,\mathrm{d}\theta \quad (4.28)
$$

$$
= \int_0^{\pi} \frac{\partial}{\partial\theta}\left(\frac{\sin\theta\,_1Y_{l0}(\theta,0)}{r_0 - ia\cos\theta} \right) \mathrm{d}\theta = 0,
$$

where we utilized

$$
_0Y_{l0}(\theta,0) = \frac{1}{\sqrt{l(l+1)}\sin\theta}\frac{\partial}{\partial\theta}\left(\sin\theta\,_1Y_{l0}(\theta,0)\right). \quad (4.29)
$$

and also

$$
\int_{-1}^{1} \left[\frac{(r_0^2 + a^2)\,_0Y_{l0}(\theta,0)}{\sqrt{l(l+1)}(r_0 - ia\cos\theta)^2} + \frac{ia\sin\theta\,_{-1}Y_{l0}(\theta,0)}{r_0 - ia\cos\theta} \right] \mathrm{d}(\cos\theta) =
$$

$$
=(l(l-1))^{-1/2} \int_{-1}^{1} {}_0Y_{l0}(\theta,0)\mathrm{d}(\cos\theta) = 0, \quad (4.30)
$$

where we utilized

$$
_{-1}Y_{l0}(\theta,0) = \frac{1}{\sqrt{l(l+1)}}\frac{\partial}{\partial\theta}\,_0Y_{l0}(\theta,0). \quad (4.31)
$$

Taking these integrals into mind the integral (4.26) reduces to

$$
2\pi \int_{-1}^{1} \left(\frac{(r_0^2 + a^2)E}{(r_0 - ia\cos\theta)^2} + \text{c.c.} \right) \mathrm{d}(\cos\theta) = 4\pi(E + \overline{E}) = 4\pi e(r_0), \quad (4.32)
$$

where
$$
E = E_a \iff r_0 < r_1 \quad E = E_b \iff r_0 > r_2.
$$

Similarly for "magnetic charges"

$$
\int_0^{2\pi} \int_0^{\pi} (-g)^{1/2} F^{*tr}\big|_{r=r_0}\,\mathrm{d}\theta\mathrm{d}\varphi = 4\pi e(r_0). \quad (4.33)
$$

We get that
$$
E - \overline{E} = 0. \quad (4.34)
$$

So finally we arrive at the solution

$$
E = \frac{1}{2}e(r_0). \quad (4.35)
$$

For a source located in the region $\langle r_1, r_2 \rangle$ with the total charge e and with zero black hole charge we get

$$
E_a = 0, \quad E_b = \frac{1}{2}e. \quad (4.36)
$$

4.1.1 The extremal case

We will repeat the previous section for the extremal black hole $a = M$. Although it is possible to take the limit $a \to 1$ in the final results from the previous section, the expression in the extremal case take a simple form so that they might be of interested when studying this special case. These results were also introduced in [2]. We start for the equation (4.14) which holds for $a = M$ as

$$(M - r)^2 \frac{d^2(^2R_{lm})}{dr^2} + \left[\frac{mM\big((2i+m)M - 2ir\big)}{(M-r)^2} - l(l+1) \right] {}^2R_{lm} = -4\pi^2 J_{lm}, \tag{4.37}$$

where now

$$^2J_{lm} = \int_0^{2\pi} \int_0^{\pi} \big(r - iM\cos\theta\big)^3 \big(r + iM\cos\theta\big) \sin\theta J_2 M^{-2} {}_{-1}\overline{Y}_{lm} \mathrm{d}\theta \mathrm{d}\varphi. \tag{4.38}$$

The equation (4.37) is most easily solved following two transformations, first consider taking

$$^2R_{lm}(x) = e^{im/x}\, {}^2y_{lm}(x), \quad x = \frac{r}{M} - 1, \tag{4.39}$$

which results in the equations

$$x^2\, {}^2y''_{lm}(x) - l(l+1)\, {}^2y_{lm}(x) - 2im\, {}^2y'_{lm}(x) = 0. \tag{4.40}$$

Further taking

$$^2y_{lm}(\chi) = x^{-l}\eta(\xi), \quad \chi = \frac{-2im}{x}, \tag{4.41}$$

results in

$$\chi\eta''(\chi) - (\chi - 2l - 2)\eta'(\chi) - l\eta(\chi) = 0. \tag{4.42}$$

The two solution of this equation are [2]

$$\eta_{lm}^{(I)} = (-2im)^{2l+1}e^{\chi}\, \chi^{-(2l+1)}\Phi(1 - l, -2l, -\chi),$$
$$\eta_{lm}^{(I)} = \Phi(l, 2l+2, \chi). \tag{4.43}$$

Where Φ is the hypergeometric cofluent function. Transforming back into y and x we get

$$^2y_{lm}^{(I)} = x^{l+1}e^{-2im/x}\Phi(1 - l, -2l, 2im/x),$$
$$^2y_{lm}^{(I)} = x^{-l}\Phi(l, 2l+2, -2im/x). \tag{4.44}$$

Further the derivation is exactly analogous to the derivation in the previous section only now $(r_+ - r_-)$ is replaced by M and a is replace by M the final forms of ϕ_i take the form

$$\phi_0|_{a=M} = \sum_{l,m} \frac{2\,a_{lm}}{l(l+1)} \exp(im/x) \frac{d^2}{dx^2} \left({}^2y_{lm}^I\right) {}_1Y_{lm}|_{a=M},$$

$$\phi_1|_{a=M} = \frac{E_a}{\varrho^2} + \frac{\sqrt{2}M}{\varrho^2} \sum_{l,m} \frac{a_{lm}}{l(l+1)} \exp(im/x) \left\{ -ia\sin\theta \frac{d}{dx} \left({}^2y_{lm}^I\right) {}_1Y_{lm} \right.$$

$$\left. + [l(l+1)]^{1/2} \left[\varrho \frac{d}{dx} \left({}^2y_{lm}^I\right) - M^2 y_{lm}^I \right] {}_0Y_{lm} \right\}|_{a=M}, \tag{4.45}$$

$$\phi_2|_{a=M} = \frac{M^2}{\varrho^2} \sum_{l,m} \alpha_{lm} \left(1 - \frac{1}{x}\right)^{-iZ_m} {}_2y_{lm}^{\mathrm{I}} {}_{-1}Y_{lm}|_{a=M}.$$

The coefficients a_{lm}, β_{lm} are now given by the formulas

$$\alpha_{lm} = \frac{4\pi}{2l+1} \int {}^2J_{lm}(\xi)\xi^{-2}\,{}^2R_{lm}^{(II)}(\xi)\mathrm{d}\xi,$$

$$\beta_{lm} = \frac{4\pi}{2l+1} \int {}^2J_{lm}(\xi)\xi^{-2}\,{}^2R_{lm}^{(I)}(\xi)\mathrm{d}\xi. \tag{4.46}$$

We've provided the derivation the full solution to the test electromagnetic field in Kerr spacetime as an infinite sum [2]. We want to inform the reader that for some specific cases, especially in the axisymmetric case, closed expressions can be found. Even more in some cases the so called Debye potential was found and the whole field can be expressed in terms of one complex scalar. A detailed discussion of the point charge in terms of Debye potential can be found in [17].

4.2   Meissner effect

By the Meissner effect, which was first introduced in [18], we understand the expulsion of magnetic fields from a superconductor. This happens when the superconductor cools below some critical temperature T_c. In GR a Meissner-like effect also arises. The test electromagnetic field are "expelled" from the horizon of extremal black hole $a = M$. Such an effect was first found noticed by Wald in [19]. The electric and magnetic flux across some region Σ can then be simplify defined as

$$i\Phi_e + \Phi_m = \int_\Sigma {}^*\mathbf{F} \tag{4.47}$$

In accordance to the Gauss theorem, such an integral over the black hole horizon would always be zero, since the black hole has zero charge. There are many ways to quantify the amount of flux coming into the black-hole. For axisymmetric fields we can intuitively take the region as the upper (or lower) hemispere. For non-axisymmetric field the construction is more complicated (see for example Bičák and Janiš [10]). We also quickly want to note that we will work in the general case $a < M$ as long as we can so that the expression may be utilized for other calculations, in the end we will take the $a \to M^-$ limit.

Writing out the integral explicitly we recover over the black hole $r = r_+$

$$i\Phi_e + \Phi_m = \int\int {}^*F_{\theta\varphi}|_{r=r_+}\mathrm{d}\varphi\mathrm{d}\theta, \tag{4.48}$$

with
$$^*F_{\theta\varphi} = \frac{a\Delta\varphi_0}{\sqrt{2}\varrho} \sin^2\theta - 2i(a^2 + r^2)\varphi_1 \sin\theta - \sqrt{2}\varrho a\varphi_2 \sin^2\theta. \qquad (4.49)$$

We now show how the integral above always behaves when we take the limit $r \to r_+$ for the axisymmetric case. To calculate these it is preferable to utilise the ingoing coordinates (1.11), in these coordinates it hold that the component (4.49) is the same $^*F_{\theta\varphi} = {}^*F_{\theta\psi}$ and schematically the integral changes to $\int_0^{2\pi} \mathrm{d}\varphi \to \int_0^{2\pi} \mathrm{d}\psi$. First we rewrite (4.45) into the coordinate ψ

$$\phi_0 = \sum_{l,m} \frac{2\,\alpha_{lm}\,{}_1Y_{lm}(\theta,\psi)}{l(l+1)x}\bigg\{ -2i(l-1)\,{}_2F_1(2-l,2+l,2-2iZ_m,x)$$

$$+ \left(1 + 2iZ_m\frac{l(x-1)+x+2iZ_m}{x-1}\right)\,{}_2F_1(1-l,2+l,2-2iZ_m,x)\bigg\},$$

$$\phi_2 = \sum_{l,m} 4\,\alpha_{lm}\,\varrho^{-2}(M^2-a^2)(x-1)x\,{}_{-1}Y_{lm}(\theta,\psi)\,{}_2F_1(1-l,2+l,2-2iZ_m,x)$$

$$\phi_1 = \sum_{l,m} \frac{2\sqrt{2}\alpha_{lm}\sqrt{M^2-a^2}}{l(l+1)\varrho^2}\bigg\{ {}_2F_1(2-l,2+l,2-2iZ_m,x)$$

$$\cdot\left[\sqrt{l(l+1)}\,\varrho\,{}_0Y_{lm}(\theta,\psi) - ia\sin\theta\,{}_1Y_{lm}(\theta,\psi)\right](x-1)(1-l)$$

$$+ \left[\sqrt{l(1+l)}{}_0Y_{lm}(\theta,\psi)\left(-4\sqrt{(M^2-a^2)}x(x-1) + (l(x-1)+x)\varrho + 2i\varrho Z_m\right)\right.$$

$$\left. + ia\sin\theta\,{}_1Y_{lm}(\theta,\psi)\,(l(x-1)+x+2iZ_m)\right]{}_2F_1(1-l,2+l,2-2iZ_m,x)\bigg\}.$$

$$(4.50)$$

When calculating limit (4.49) we cannot just take the limits of φ_i but we need to take into account the whole equations (4.49). From rudimentary analysis it is the general knowledge that a sum of limits is a limit of sums if both limits exist and are finite. Similarly for product, a limit of a product of functions is a product of limits when both limits exist, are finite and non-zero. Taking this into account we can split (4.49) into the expressions

$$\lim_{r\to r_+}\Delta\phi_0 = \sum_{l,m} \frac{16\alpha_{lm}(a^2-M^2)}{l(l+1)} Z_m(2Z_m - i){}_1Y_{lm}(\theta,\psi)$$

$$\cdot\,{}_2F_1(1-l,2+l,2-2iZ_m,1),$$

$$\lim_{r\to r_+}\phi_1 = \sum_{l,m} \frac{2\sqrt{2}\alpha_{lm}\sqrt{M^2-a^2}}{l(1+l)(r_+ - ia\cos\theta)^2}(2Z_m - i)\,{}_2F_1(1-l,2+l,2-2iZ_m,1)$$

$$\cdot\bigg\{\sqrt{l(l+1)}\left[iM + \sqrt{(M^2-a^2)} + a\cos\theta\right]{}_0Y_{lm}(\theta,\psi)$$

$$+ a\sin\theta\,{}_1Y_{lm}(\theta,\psi)\bigg\},$$

$$\lim_{r\to r_+}\phi_2 = 0.$$

$$(4.51)$$

In the first we had to take $\Delta\phi_0$ since the product rule for limits doesn't hold. Finally, after a straightforward simplification we can explicitly write out (4.49)

$$
{}^*F_{\theta\psi}|_{r=r_+} = \sum_{l,m} \frac{8\sqrt{2}\,\alpha_{lm}\sin\theta}{l(l+1)\varrho_+^2}(2Z_m - i)\,{}_2F_1(1-l, 2+l, 2-2iZ_m, 1)
$$
$$
\left\{ \sqrt{l(l+1)}(M^2 r_+ - Ma^2)\varrho_+\,{}_0Y_{lm}(\theta,\psi) + (Ma^3 i - iM^2 r_+^2 \right. \tag{4.52}
$$
$$
\left. -(M^2 - a^2)\varrho_+ Z_m)\sin\theta\,{}_1Y_{lm}(\theta,\psi) \right\},
$$

where we denoted $\varrho_+ = \varrho|_{r=r_+} = r_+ - ia\cos\theta$. Directly from the expression above we can prove the Meissner effect. For stationary axially symmetric sources $J^i = J^i(r,\theta)\ \forall i \in \{0,1,2,3\}$ and for the extremal black hole $a = M$ the integral (4.15) over the variable φ reduces to integral over the spherical harmonic, then further considering (4.25) we get

$$
\int_0^{2\pi} {}_{-1}\overline{Y}_{lm}(\theta,\varphi)\mathrm{d}\varphi = {}_{-1}\overline{Y}_{lm}(\theta,0)2\pi\delta_{m,0} \implies \alpha_{lm} = \alpha_{l0}\delta_{m,0}. \tag{4.53}
$$

For these types of sources we get

$$
\lim_{\substack{x\to 1^+ \\ a\to M}} {}^*F_{\theta\psi}|_{\alpha_{lm}=\alpha_{l0}\delta_{m,0}} = 0 \tag{4.54}
$$

We thus recovered the expulsions of electromagnetic axisymmetric fields for extremal black holes. So the Meissner effect says that locally the electromagnetic flux at the horizon of any vacuum axisymmetric stationary solution of the Maxwell equation is zero. This also implies that, for the extremal Kerr black hole, the flux across the lower (or upper) hemisphere of any stationary electromagnetic solution is zero. Since for any field we can formally split it into two parts, the part perpendicular to axis of symmetry $\mathbf{F}^\perp$ and the part parallel to axis of symmetry $\mathbf{F}^\parallel$. The former part has of course zero total flux across the horizon, this is given by the symmetry of the problem, for the latter the Meissner effect holds.

We now shortly discuss the history and relevance of the Meissner effect.

History

It would be cumbersome to provide an exhaustive list of all articles discussing the Meissner effect, we thus just the outline of the most important developments in Meissner effect. The history of the Meissner effect begins with the Wald's solution [19], where they first derived the homogeneous magnetic field aligned along the symmetry axis of a rotating black hole. They have done this by noticing that a combination of the axial and timelike Killing vectors generates this solution. Later King [20] noticed that flux across the lower hemisphere of this solution goes to zero as the black hole becomes extremal $a \to M$. In 1976 Bičák and Dvořák [2] showed that this is the case for any axially symmetric test electromagnetic field proving it in a similar fashion to the proof given above. More recent developments have been in numerical methods for general relativistic magnetohydrodynamics, such have been done in for example [21].
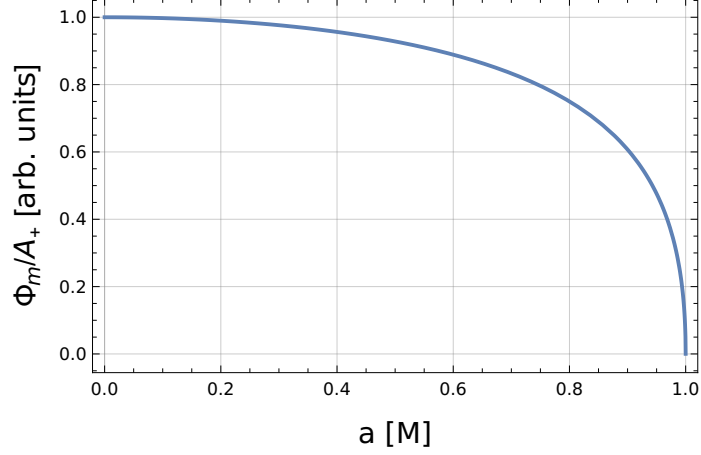
Figure 4.1: The and magnetic Φ_m flux across the lower horizon of the Kerr black hole of the homogeneous magnetic field of the homogeneous magnetic field 5.5. The flux is divided by the black hole area $A_+ = 4\pi(r_+^2 + a^2)$. We can see the Meissner effect starts to prevail at large values of a.

Relevance

The Meissner effect isn't some artifact of the extremal case. This is because the flux behaves in a continuous manner as $a \to M$. This can be seen in 4.1. Thus the Meissner effect is surely important to understanding the fundamental physics behind the "expulsion" of electromagnetic fields which is yet not understood, although it has been discussed in many articles like [22]. There is an ongoing discussion about wether significantly reduce or even eliminate the Blandford-Znajek mechanism. For a detailed discussion we refer the reader to [23, 24]. The Meissner effect was found to be true in more general metrics like the Magnetized Kerr-Newman one discussed in [25].

4.3 Invariants

We already defined the electromagnetic invariants and explained their meaning in Section 3. To calculate these invariants at horizons we express the Maxwell tensor **F** in terms of the NP tetrad (2.31) while keeping in mind the normalization of the tetrad (2.15) and (2.16). Using these we get after a long but straightforwards simplification

$$\frac{1}{4}F^{\alpha\beta}F_{\alpha\beta} = \phi_0\phi_2 + \overline{\phi}_0\overline{\phi}_2 - \phi_1^2 - \overline{\phi}_1^2,$$

$$\frac{1}{4}F^{\alpha\beta} \star F_{\alpha\beta} = \left(\phi_1^2 - \overline{\phi}_1^2 - \phi_0\phi_2 + \overline{\phi}_0\overline{\phi}_2\right)\epsilon_{\alpha\beta\gamma\iota}l^\alpha n^\beta m^\gamma \overline{m}^\iota \qquad (4.55)$$

$$= i\left(\phi_1^2 - \overline{\phi}_1^2 - \phi_0\phi_2 + \overline{\phi}_0\overline{\phi}_2\right).$$

The scalar $\epsilon_{\alpha\beta\gamma\iota}l^\alpha n^\beta m^\gamma \overline{m}^\iota$ is best calculated in the NP basis.

We now consider an axially symmetric test electromagnetic field. According to [10] the NP components at horizon ($\Delta = 0$) for the extremal Kerr black hole ($a = M$) behave as

$$\phi_0 \sim \Delta^{(l-1)/2}, \; \phi_1 \sim \Delta^{l/2}, \; \phi_2 \sim \Delta^{(l+1)/2}. \qquad (4.56)$$

27

Reordering the sums in (4.55) we get

$$
\begin{aligned}
\frac{1}{2} F^{\alpha\beta} F_{\alpha\beta}|_{(a=M,\Delta=0)} &= 0, \\
\frac{1}{4} F^{\alpha\beta} \star F_{\alpha\beta}|_{(a=M,\Delta=0)} &= 0.
\end{aligned}
\tag{4.57}
$$

Thus, in the context of axisymmetric test fields surrounding an extremal Kerr black hole, the magnitudes of magnetic and electric fields become equal at the horizon $||\mathbf{B}||^2 = ||\mathbf{E}||^2$, and the two fields are perpendicular to each other $\mathbf{E}\cdot\mathbf{B}=0$, this does not hold for the non-extremal case and can be formulated in terms of a single invariant as

$$
\lambda_1|_{a=M,\Delta=0} = 0.
\tag{4.58}
$$

5. Fields lines and visualization

Before discussing the source term we will take a short detour and discuss visualization of Electromagnetic fields in GR. The electric and magnetic field lines are defined as tangent to the Lorentz force.

$$\frac{\mathrm{d}x^\mu}{\mathrm{d}s} = E^\mu \quad \frac{\mathrm{d}x^\mu}{\mathrm{d}s} = B^\mu. \tag{5.1}$$

These vector fields are not what the local observer measures. The local observer measures the projection of these fields onto it's own tetrad $\{\mathbf{e}_i\}_{i=0,1,2,3}$, $\mathbf{e}_0 = \mathbf{u}$. As before we denote the projection of vector fields with the bracketed indices we have the relations

$$B^{(a)} = -\mathbf{e}_\mu^{(a)} \star F^{\mu\nu} u_\nu = - \star F^{(a)(t)},$$
$$E^{(a)} = \mathbf{e}_\mu^{(a)} F^{\mu\nu} u_\nu = F^{(a)(t)}. \tag{5.2}$$

The relation between the vector field projected onto a tetrad and the coordinate one is

$$B^\mu = -\star F^\mu{}_\nu u^\nu = e^\mu_{(k)} B^{(k)},$$
$$E^\mu = F^\mu{}_\nu u^\nu = e^\mu_{(k)} E^{(k)}. \tag{5.3}$$

Instead of integrating the field lines on the manifold and then projecting these integral curves onto a flat plane for purposes of visualization we can identify the orthogonal projection with the flat plane and find the integral curves there. This has the advantage that the field lines are as they would be measured by the local observer. This can be more physically appropriate for some applications.

We define the field lines for the orthogonal projections as

$$\frac{\mathrm{d}x^{(a)}}{\mathrm{d}s} = \frac{E^{(a)}}{h_a}, \quad \frac{\mathrm{d}x^{(a)}}{\mathrm{d}s} = \frac{B^{(a)}}{h_a}. \tag{5.4}$$

we have included polar (or spherical) Lamé coefficients h_a, we do not sum over a or (a). For an orthogonal frame the Lorentz force is obviously tangent to the field lines.

We discuss the differences between the tetrad field lines and the coordinate ones in the section below after introducing the homogeneous magnetic field.

5.1 Homogeneous magnetic field at infinity

Since we are dealing with perturbations the magnetic field doesn't affect the geometry, on the other hand the geometry affects the field. A field that would be homogeneous everywhere in Minkowski's space ($a = 0, M = 0$) to be homogeneous only at infinity. Furthermore near the horizon of black hole the geometry "induces" a electric field from a purely magnetic field at infinity.

The full form of magnetic field homogeneous at infinity was given in [2]. Let us consider asymptotically, at large distances, Minkowskian coordinates $\{x =$

$r \sin\theta \cos\varphi, y = r \sin\theta \sin\varphi, z = r \cos\theta\}$, in these coordinates the field takes the asymptotical form $B_x = B \sin\alpha, B_z = B \cos\alpha, B_y = 0$. Without any loss of generality we took $B_y = 0$, we also later parameterized the field by it's magnitude B and the angle from the z-axis α.

The electromagnetic field tensor then has the asymptotical form $(r \to \infty)$[2].

$$
\begin{aligned}
F^{tr} &= F^{t\theta} = F^{t\varphi} = 0, \\
F^{r\theta} &= -\frac{\sin\varphi}{r} B \sin\alpha, \\
F^{r\varphi} &= \frac{B}{r} \left(\cos\alpha - \cot\theta \cos\varphi B \sin\alpha \right), \\
F^{\theta\varphi} &= \frac{B}{r^2} \left(\cot\theta \cos\alpha + \cos\varphi \sin\alpha \right).
\end{aligned}
\tag{5.5}
$$

From comparing the asymptotic form of (4.45) and (5.5) we get that the only nonzero coefficients are

$$
a_{11} = i\sqrt{\frac{\pi}{6}} B \sin\alpha, \quad a_{10} = i\sqrt{\frac{\pi}{3}} B \cos\alpha, \quad a_{1-1} = -i\sqrt{\frac{\pi}{6}} B \sin\alpha.
\tag{5.6}
$$

Writing out explicitly the scalars (4.45) while reparametrizing by the angle from the z-axis α and the magnitude of the field B: $B_0 = B \cos\alpha, B_1 = B \sin\alpha$

$$
\begin{aligned}
\phi_0 &= \frac{B}{\sqrt{2}} \left\{ \frac{\sin\alpha}{2\Delta(\overline{\varrho} - 2r)} \left[\cos\psi \left(4Ma\overline{\varrho} + a\Delta\left(3 - \cos(2\theta)\right) + 2i\Delta \cos\theta r \right) \right. \right. \\
&\quad + 2\left(-2M\Sigma + \Delta(\overline{\varrho} - 2r) + 2\left(\Sigma + M(\overline{\varrho} - 2r)\right)r \right) \sin(\psi) \right] + i\cos\alpha \sin\theta \Big\} \\
\phi_1 &= B \left\{ \frac{i\cos\alpha\Delta \sin\theta}{\sqrt{2}(2\Sigma - 4\overline{\varrho}r)} + \frac{i\sin\alpha \sin\theta}{2\left(\Sigma + 2(\overline{\varrho} - 2r)r\right)} \left[\cos\psi \left((\overline{\varrho} - 2r)r + M(-\overline{\varrho} + r) \right) \right. \right. \\
&\qquad\qquad\qquad\qquad\qquad\qquad\qquad\qquad\qquad\qquad \left. \left. + a(M - \overline{\varrho} + 2r) \sin\psi \right] \right\}, \\
\phi_2 &= -B \left\{ \frac{\cos\alpha \left(a\left(3 + \cos(2\theta)\right)(M - r) - 2i\cos\theta a^2 + r^2 \right)}{4(\overline{\varrho} - 2r)^2} \right. \\
&\quad + \frac{i\cos\alpha \left\{ \cos\psi \left[(\overline{\varrho} - 2r)r + M(-\overline{\varrho} + r) \right] + a(M - \overline{\varrho} + 2r) \sin\psi \right\} \sin\theta}{2\left(\Sigma + 2(\overline{\varrho} - 2r)r\right)} \right\}.
\end{aligned}
\tag{5.7}
$$

with $\varrho = r - ia\cos\theta$ as before and ψ being the Kerr ingoing coordinate.

$$
\psi = \frac{a}{r_+ - r_-} \ln\left(\frac{r - r_+}{r - r_-} \right) + \varphi.
$$

We do not provide the full form of the tensor **F** since the field is more elegantly described in terms of the NP scalars, but for the convenience of the reader we have expressed the tensor **F** in terms of the NP scalars in Boyer-Lindquist coordinates along with projections to the tetrad fields in the appendix A.2.

Since we have several visualization techniques we split the discussion into the field aligned with the axis of symmetry. Such field is probably the most

astrophysically relevant, the direction of the field will eventually be the same as of the axis of symmetry, but since the time it would take to align both directions is probably long [2], the oblique case is also of interest.

Aligned field

The field is aligned with the axis of symmetry for $\alpha = 0$. As we discussed in above we have a plethora of ways to visualize the electromagnetic fields. Different visualization techniques are shown in Fig. 5.1 reveal significant discrepancies. We will now attempt to summarize the field behaviour for different observers.

The ZAMO coordinate field lines exhibit expulsion of the field lines for the extremal case $a = M$. As anticipated as we approach the horizon ($r = r_+$) the angle of approach of the field lines diverges, signifying a complete expulsion of the electromagnetic field from the horizon. Consistently with this expulsion both the electric and magnetic field completely vanishes at the horizon $r = r_+$.

However, the ZAMO tetrad field lines present a contrasting view. The field lines do no exhibit any expulsion at all. The angle of approach remains finite as we approach the horizon. Perhaps in accordance with the Meissner effect the electric and magnetic field also completely vanish at the horizon. This view agrees with the behaviour of the norm of the magnetic field $||\mathbf{B}||$ shown in fig. 5.2.

For the Doran observer coordinate and tetrad field lines experience some expulsion at the horizon. However this expulsion does not strictly adhere to the Meissner effect. Here the field remains non-zero at the horizon and the situation is more subtle, if we zoom in on the horizon we can see that some of the tetrad field lines start at the horizon and then plunge back in Fig. 5.3. Such field lines start to appear at around $a \approx 0.9M$. The coordinate field lines for the Doran observer stay strictly at the horizon, since B^r is zero everywhere at the horizon. As can be seen in Fig. 5.2 the norm of the magnetic field $||\mathbf{B}||$on the horizon is not zero as in the ZAMO case.

We also show the electric field lines Fig. 5.4, since these are subordinate to the magnetic field lines, we plot just the field lines for the Doran observer. And we also projected the ZAMO tetrad field lines on the embedding in the figure Fig. 5.6.

Finally we also note another difference between the ZAMO and Doran observer, for ZAMO observer the tetrad fields stay at constant φ, this is because the ZAMO observer corotates in a natural way around the Black hole. But the Doran observers move at constant φ so the field lines are shifted in this direction as can be seen in Fig. 5.7.

To summarize the Meissner effect, if formulated as expulsion of field lines from the black hole horizon in the extremal black hole case, seems to be coordinate dependent effect. Different observer and different visualization techniques display different levels of expulsion from the horizon, even thought it always stays true that the flux through the black hole Fig. 4.54 and Fig. 4.57 electromagnetic invariants vanish. Thus the Meissner effect should not be formulated as expulsion of the magnetic/electric field lines, but should stay strictly confined to the vanishing flux or invariants, even thought this is not intuitive from the point of classical electrodynamics.

Oblique field

The oblique field $\alpha = \pi/2$ can really only be sensibly visualized as 2D graph in the $\theta = \pi/2$ plane, since the field lines starting in this plane stay confined to this plane. The Meissner effect is completely gone since it's experienced only for aligned fields. We here only quickly note that since the field is dependent on the coordinate φ it is important to utilize some other well behaved coordinate as the coordinate φ winds infinitely around the horizon. This is visualized in Fig. 5.5. As noted in [26] for ZAMO observer there exist closed loops of magnetic lines which start at the horizon and end at the horizon. For the Doran observer the field lines coming from infinity can either hit the horizon. Or can continue past the black hole. There exist no closed magnetic loops as in the ZAMO case.

(a) ZAMO coordinate field lines

(b) Doran coordinate field lines

(c) ZAMO tetrad field lines

(d) Doran tetrad field lines
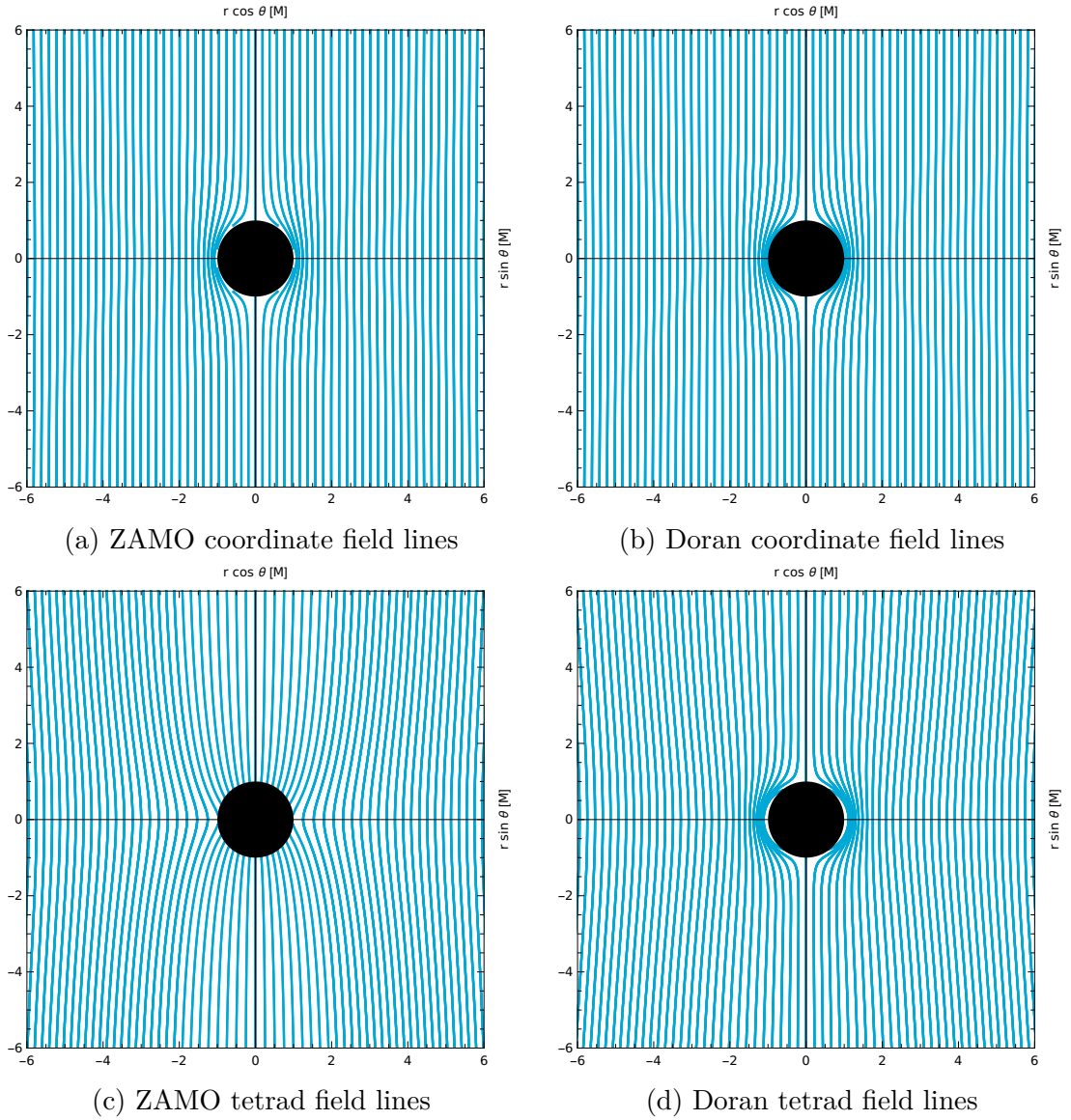
Figure 5.1: Comparison of two different visualization techniques for field lines of homogeneous magnetic field for $a = M$. We can see substantial difference. Especially for the ZAMO observer, for which field lines as measured by the local observer (tetrad field lines) actually "hit" the black hole.
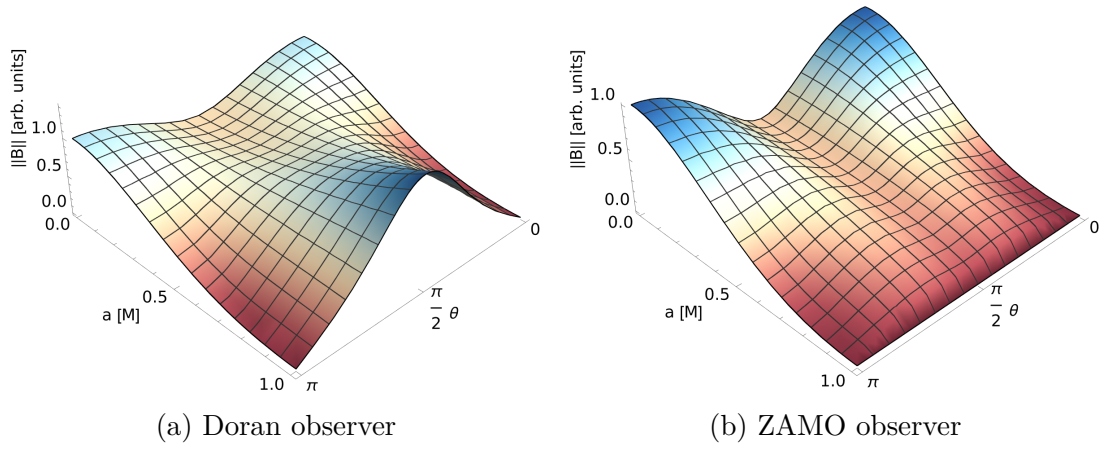
(a) Doran observer

(b) ZAMO observer

Figure 5.2: Norms of the magnetic field $||\mathbf{B}||$ at the horizon $r = r_+$ plotted with respects to the rotation of the black hole a and the coordinate θ.
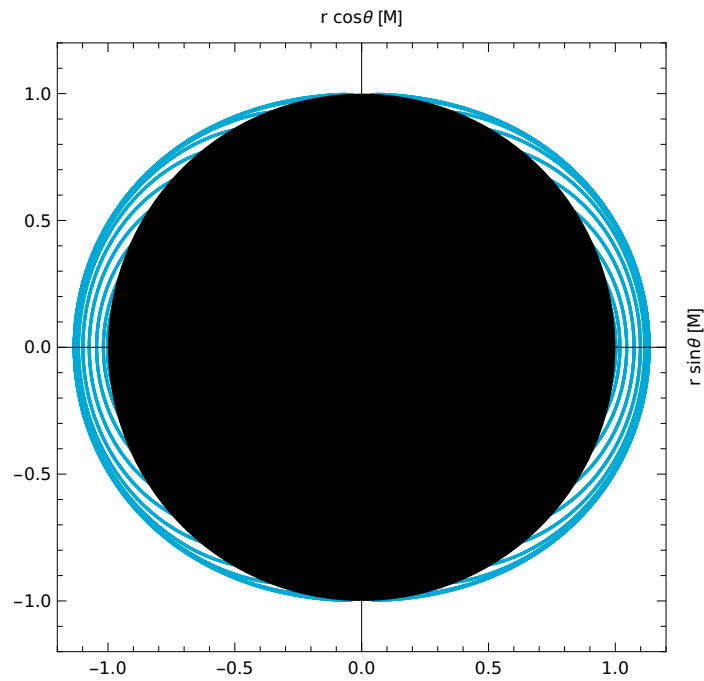
Figure 5.3: Field lines which start at the horizon for the tetrad Doran observer $a = M$.

(a) Doran tetrad field lines   (b) Doran coordinate field lines
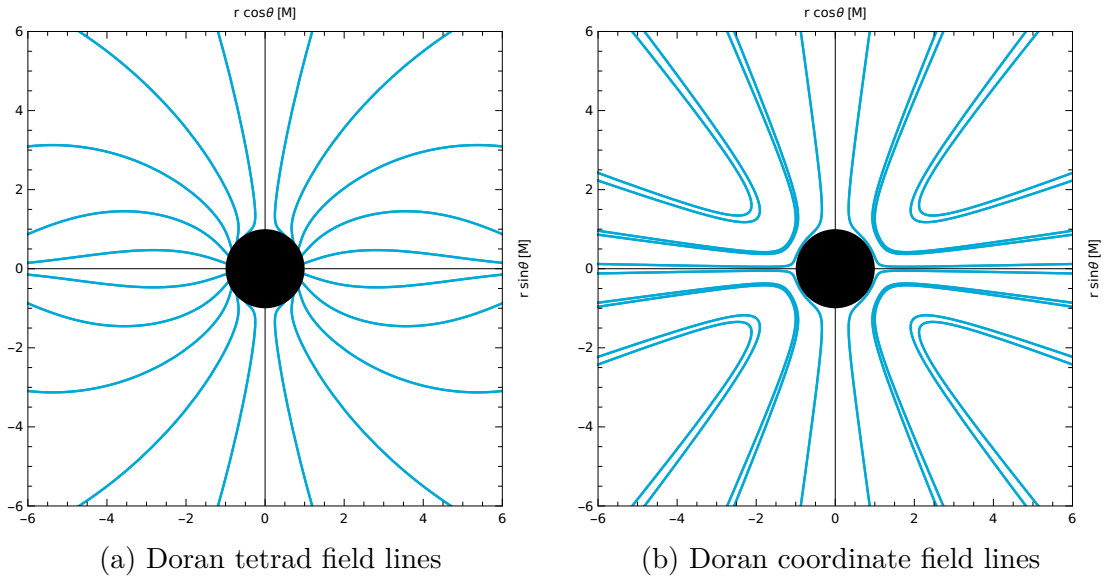
Figure 5.4: Visualization of induced electric field for the extremal Kerr black hole $a = M$.
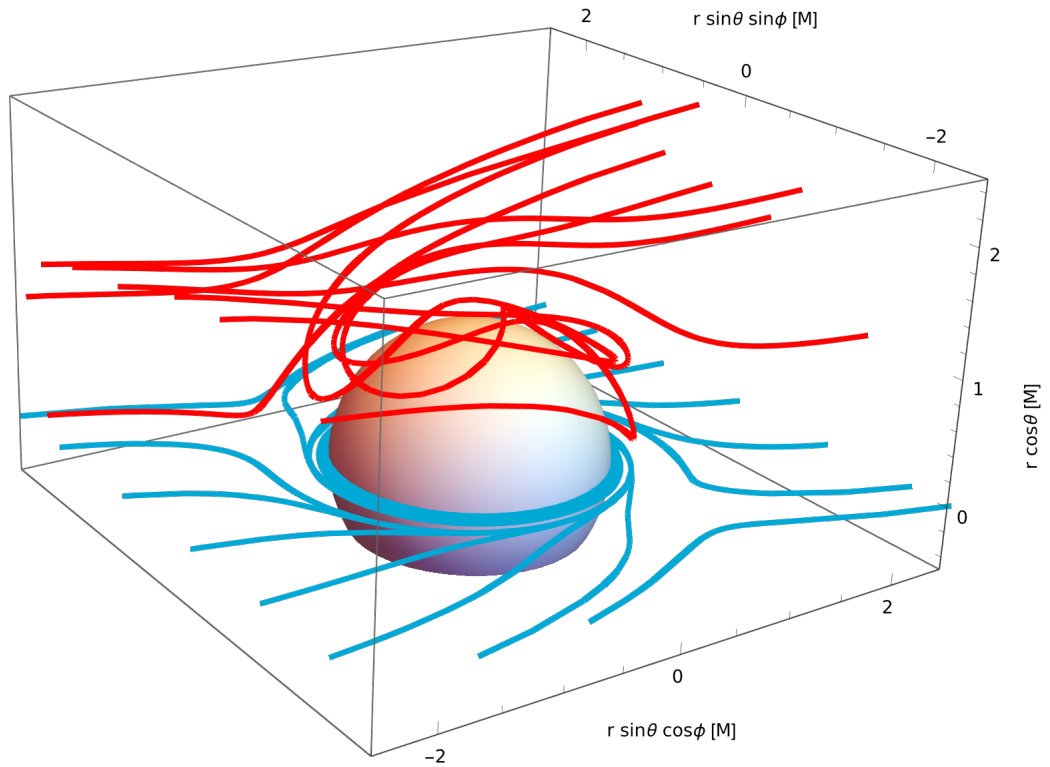
Figure 5.5: Oblique field $a = 0.998M$ ZAMO Tetrad field lines, magnetic field lines starting at $\pi/2$ are blue, mag field lines at $\pi/4$ are red. We can see the infinite winding effect of the φ coordinate.
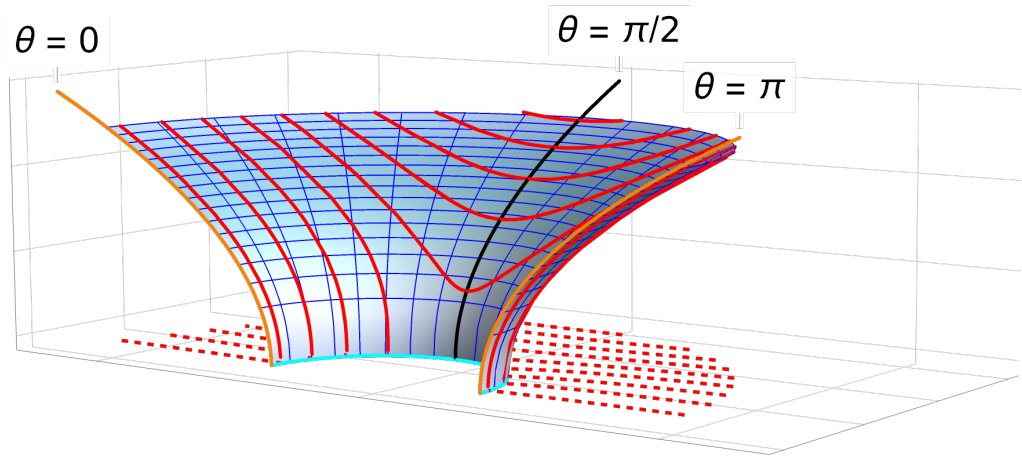
Figure 5.6: Magnetic field lines (red) of Homogeneous magnetic field aligned with the axis of symmetry for orthogonal ZAMO magnetic field projected onto the embedding of Kerr black hole $a = 1/2M$ into $\mathbb{E}^3$. The curves are also projected onto the flat $x - z$ plane (dashed).
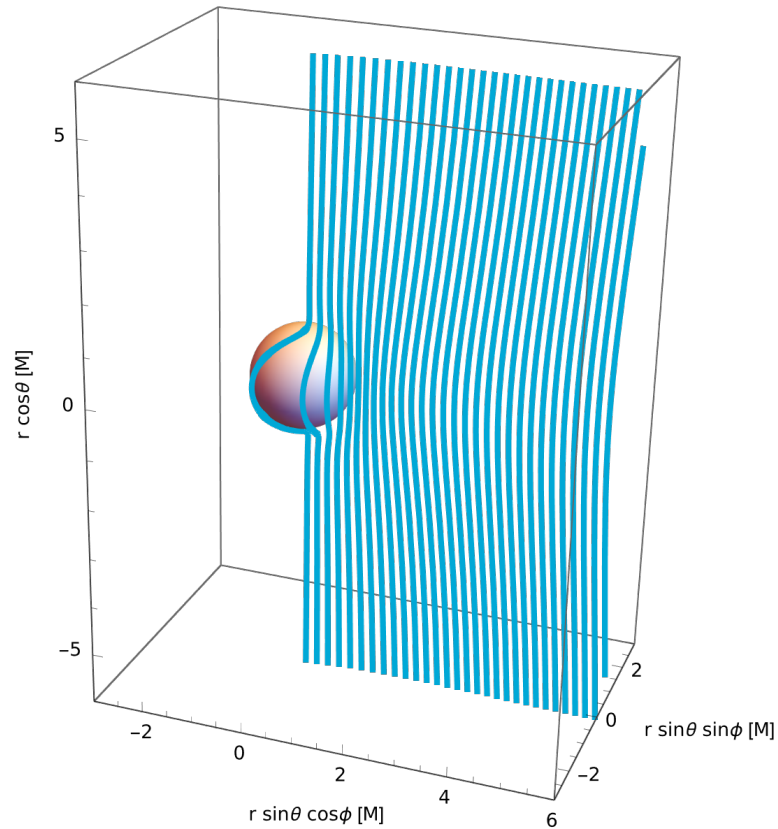

Figure 5.7: Full 3D plot of the magnetic field lines projected onto the Doran observer tetrad. For the extremal Kerr black hole $a = M$. Only a few lines starting at $r \cos \theta = 2$ are shown for the sake of clarity.
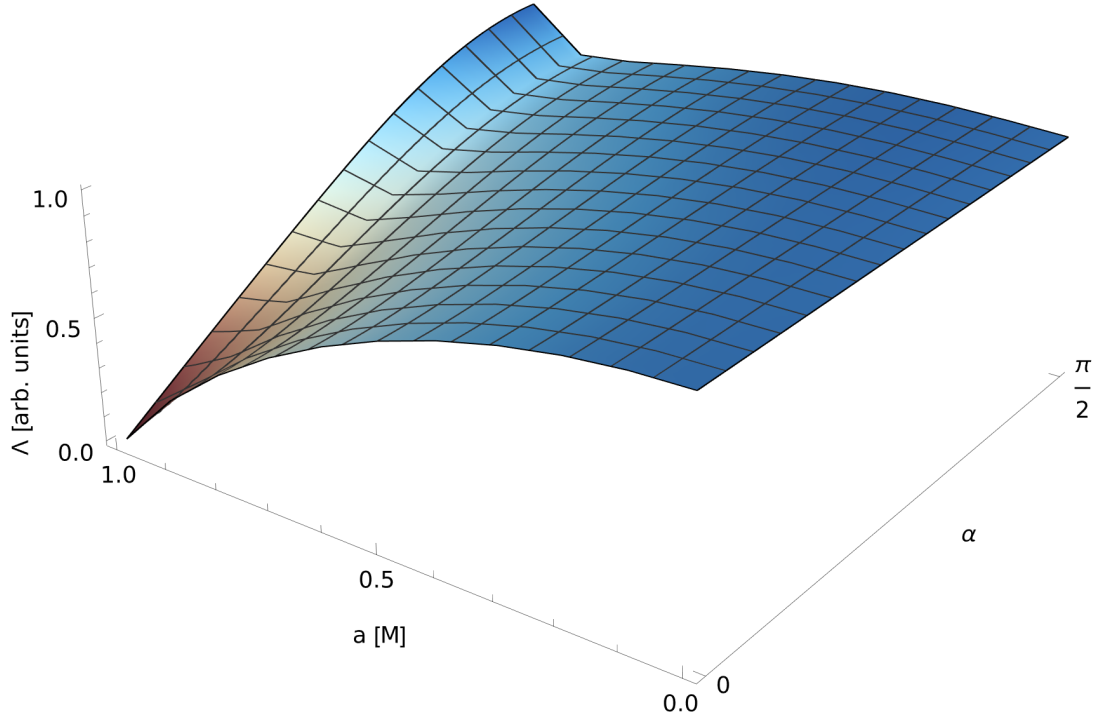
Figure 5.8: Λ function on the black hole horizon $r = r_+$ of the homogeneous magnetic field parameterized by the angle of the field to the axis of symmetry α and the rotational parameter of the black hole a. Qualitatively, the graph is similar to the homogeneous magnetic field.

To visualize how the Meissner effect depends on the direction of the homogeneous magnetic field we then take the eigenvalue λ_1 and integrate it over the whole black-hole we get a function Λ that is dependent on α and the rotation parameter a.

$$\Lambda(\alpha, a) = \int_0^{2\pi} \int_0^{\pi} \lambda_1 \Sigma \sin\theta \, \mathrm{d}\theta \, \mathrm{d}\varphi. \tag{5.8}$$

The function behaviour can be seen in Fig. 5.8. We can clearly see how the field becomes null for the extremal black hole $a = M$ and the aligned field $\alpha = 0$.

6. Source terms and fields

In this section we describe the source terms while also deriving the coefficients α_{lm}, β_{lm}. We first start with the simplest case, the point charge, these have been already derived in [2]. Then we will move to a charged axial loop which we later generalize into a non-axial loop and a disk.

Any source must of course satisfy the continuity equation

$$\nabla_\mu J^\mu = \frac{1}{(-g)^{1/2}} \frac{\partial}{\partial x^\mu} \left((-g)^{1/2} J^\mu \right) = 0, \tag{6.1}$$

with $(-g)^{1/2} = \Sigma \sin\theta$ being the metric determinant in Boyer-Lindquist coordinates. The same equation holds for the magnetic current vector M^μ.

6.1   Point charge

The simplest non-axially symmetric source is the point charge. A point charge at the point r_0, θ_0, φ_0 is described by the following expression in Boyer-Lindquist coordinates

$$\mathbf{J} = \frac{e}{\Sigma_0 \sin\theta_0} \boldsymbol{\partial}_t \, \delta(r - r_0)\delta(\theta - \theta_0)\delta(\varphi - \varphi_0). \tag{6.2}$$

Following steps derived in Section 4.1 we then calculate

$$
\begin{aligned}
{}^2 J_{lm} = {}& e\Delta \left[2\sqrt{2}(r_+ - r_-)^2 \overline{\varrho}_0 \right]^{-1} \left\{ ia\sin\theta_0 \, {}_{-1}\overline{Y}_{lm}(\theta_0, \varphi_0)\delta'(r - r_0) \right. \\
& \left. + \left[\frac{am}{\Delta_0} \sin\theta_0 \, {}_{-1}\overline{Y}_{lm}(\theta_0, \varphi_0) - \sqrt{l(l+1)} \, {}_0\overline{Y}_{lm}(\theta_0, \varphi_0) \right] \delta(r - r_0) \right\}.
\end{aligned}
\tag{6.3}
$$

Employing (4.25) we get

$$
\begin{aligned}
a_{lm} = {}& \frac{2\pi e}{\sqrt{2}\,(r_+ - r_-)(r_0 + ia\cos\theta_0)} \frac{(l+1)!\Gamma\left(l+1-2iZ_m\right)}{(2l+1)!\Gamma\left(2-2iZ_m\right)} \left(1 - \frac{1}{x_0}\right)^{-iZ_m} \\
& \cdot (-x_0)^{-l} \left\{ -\frac{ia}{r_+ - r_-} \sin\theta_0 \overline{Y}_{lm}(\theta_0, \varphi_0) \frac{l}{x_0} F(l+1, l+1 \right. \\
& -2iZ_m, 2l+2; x_0^{-1}) + [l(l+1)]^{1/2} \overline{Y}_{lm}(\theta_0, \varphi_0) \\
& \left. \cdot F\left(l, l+1-2iZ_m, 2l+2; x_0^{-1}\right) \right\}, \\
b_{lm} = {}& \frac{2\pi e}{\sqrt{2}\,(r_+ - r_-)(r_0 + ia\cos\theta_0)} \frac{(l+1)!\Gamma\left(l+1-2iZ_m\right)}{(2l+1)!\Gamma\left(2-2iZ_m\right)} \left(1 - \frac{1}{x_0}\right)^{iZ_m} \quad (6.4) \\
& \cdot \left[-\frac{ia}{r_+ - r_-}(1 - 2iZ_m)\sin\theta_0 \overline{Y}_{lm}(\theta_0, \varphi_0) \right. \\
& \cdot F\left(l+1, -l, 1-2iZ_m; x_0\right) + [l(l+1)]^{1/2}\overline{Y}_{lm}(\theta_0, \varphi_0) x_0(x_0 - 1), \\
& \left. \cdot F\left(l+2, 1-l, 2-2iZ_m; x_0\right) \right] \\
E_a = {}& 0, \quad E_b = \frac{1}{2}e.
\end{aligned}
$$

Here we want to note that again for axisymmetric case $\theta_0 = 0, \varphi_0 = 0$ only the modes with $m = 0$ are non-zero.

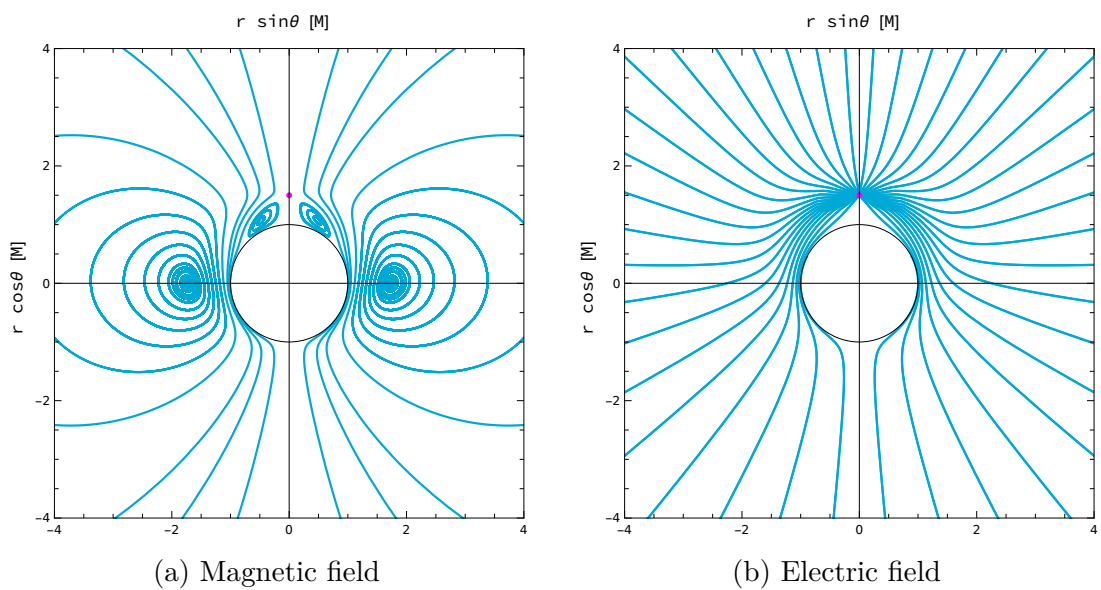(a) Magnetic field   (b) Electric field

Figure 6.1: Magnetic and electric coordinate fields lines with respect to the ZAMO observer for the extreme Kerr black hole ($a = M$). The charge is located at $r = 3/2M$ and is visualized magenta, the outer horizon r_+ is visualized black. No truncation error can be seen because we've used the closed form derived in [17].

6.2 Axial current loop

Consider an current loop in the equatorial plane lying at $\theta = \pi/2$, $r = r_0 > r_+$. We will consider a axial current loop with the charge q and the current I as measured by the ZAMO observers. To relate these quantities to the four-vector J^μ we consider the form.

$$\mathbf{J} = \left(\frac{q}{2\pi\Sigma_0} \boldsymbol{\partial}_t + C\boldsymbol{\partial}_\varphi \right) \delta(r - r_0)\delta(r - \pi/2). \tag{6.5}$$

In ZAMO coordinates this the third component four-vector has the form

$$J^\varphi_{ZAMO} = \sqrt{\frac{A_0}{\Delta_0}} r_0 \left[C - \frac{Mae}{\pi r_0 A_0} \right] \delta(\xi^r - \xi^r_0)\delta(\xi^\theta - \xi^\theta_0). \tag{6.6}$$

The observer meassure the current as

$$J^\varphi_{ZAMO} = I\delta(\xi^r - \xi^r_0)\delta(\xi^\theta - \xi^\theta_0). \tag{6.7}$$

We can relate

$$C = r_0^{-1} \left[\frac{Maq}{\pi A_0} + I\sqrt{\frac{\Delta_0}{A_0}} \right]. \tag{6.8}$$

where we denoted $\Delta_0 = \Delta_{|r=r0}, \Sigma_0 = \Sigma_{|r=r_0,\theta=\theta_0}, A_0 = A_{|r=r_0,\theta=\theta_0}$.

From (4.16) we then find

$$^2J_{lm} = {}^2J^R_{lm} + {}^2, J^L_{lm} \tag{6.9}$$

with

$$
\begin{aligned}
^2J^R_{lm} &= \frac{e\Delta\delta_{m0}}{2\sqrt{2}r_0(r_+ - r_-)^2} \Big\{ ia \;_{-1}\overline{Y}_{l,m}(\pi/2,0)\delta'(r - r_0) \\
&\quad - (l(l+1))^{1/2} \;_0\overline{Y}_{lm}(\pi/2,0)\delta(r - r_0) \Big\}, \\
^2J^L_{lm} &= -\frac{\Delta\delta_{m0}}{\sqrt{2}(r_+ - r_-)^2} \left[(Mae/A_0) + \pi I(\Delta_0/A_0)^{1/2} \right] \\
&\quad \Big[i(r_0^2 + a^2)_{-1}\overline{Y}_{lm}(\pi/2,0)\delta'(r - r_0) \\
&\quad + \Big\{ ir_0 \;_{-1}\overline{Y}_{lm}(\pi/2,0) - a((l+1))^{1/2} \;_0\overline{Y}_{lm}(\pi/2,0) \Big\} \delta(r - r_0) \Big].
\end{aligned}
\tag{6.10}
$$

The splitting of (6.9) is in correspondence to different physical situations. For static charged axial ring with no current $^2J^C_{lm} = {}^2J^L_{lm}$, for a current loop with no charge $^2J_{lm} = {}^2J^L_{lm}, e = 0$. For a current loop with charge have the consider the whole equations (6.9).

From equation (4.25) and following the notation above we get

$$
\begin{aligned}
\alpha_{lm} &= \alpha^R_{lm} + \alpha^L_{lm}, \\
\beta_{lm} &= \beta^R_{lm} + \beta^L_{lm},
\end{aligned}
\tag{6.11}
$$

with

$$a_{lm}^R = \frac{\delta_{m0} 2\pi e}{\sqrt{2}\,(r_+ - r_-)\,(r_0 + ia\cos\theta_0)} \frac{(l+1)!\,l!}{(2l+1)!}\,(-x_0)^{-l}$$

$$\cdot \left\{ -\frac{ia}{r_+ - r_-} \sin\theta_{0\,-1}\bar{Y}_{l0}(\theta_0, 0)\frac{l}{x_0} F\left(l+1, l+1, 2l+2; x_0^{-1}\right) \right.$$

$$\left. + [l(l+1)]^{1/2}\bar{Y}_{l0}(\theta_0, 0)\, F\left(l, l+1, 2l+2; x_0^{-1}\right) \right\},$$

$$b_{lm}^R = \frac{\delta_{m0} 2\pi e}{\sqrt{2}\,(r_+ - r_-)\,(r_0 + ia\cos\theta_0)} \frac{(l+1)!\,l!}{(2l+1)!}$$

$$\cdot \left\{ -\frac{ia}{r_+ - r_-} \sin\theta_0 - 1\bar{Y}_{l0}(\theta_0, 0)\, F\left(l+1, -l, 1; x_0\right) + [l(l+1)]^{1/2} \right.$$

$$\left. \cdot\bar{Y}_{l0}(\theta_0, 0)\, x_0\,(x_0 - 1)\, F\left(l+2, 1-l, 2; x_0\right) \right\},$$

$$E_a = 0, \quad E_b = \frac{1}{2}e. \tag{6.12}$$

and

$$a_{lm}^L = \frac{\delta_{m0} 4\pi}{\sqrt{2}\,(r_+ - r_-)} \frac{(l+1)!\,l!}{(2l+1)!}\left[Mae/A_0 + \pi I\,(\Delta_0/A_0)^{1/2}\right](-x_0)^{-l}\left[i\frac{r_0^2 + a^2}{r_+ - r_-}\right.$$

$$\cdot\,_{-1}\bar{Y}_{l0}\left(\frac{\pi}{2}, 0\right)\frac{l}{x_0} F\left(l+1, l+1, 2l+2; x_0^{-1}\right) + \left\{ir_{0\,-1}\bar{Y}_{l0}\left(\frac{\pi}{2}, 0\right)\right.$$

$$\left.\left. -a[l(l+1)]^{1/2}\bar{Y}_{l0}\left(\frac{\pi}{2}, 0\right)\right\} F\left(l, l+1, 2l+2; x_0^{-1}\right)\right],$$

$$b_{lm}^L = \frac{\delta_{m0} 4\pi}{\sqrt{2}\,(r_+ - r_-)} \frac{(l+1)!\,l!}{(2l+1)!}\left[Mae/A_0 + \pi I\,(\Delta_0/A_0)^{1/2}\right]\left[i\frac{r_0^2 + a^2}{r_+ - r_-}\bar{Y}_{l0}\left(\frac{\pi}{2}, 0\right)\right.$$

$$\cdot\, F\left(l+1, -l, 1; x_0\right) + \left\{ir_{0\,-1}\bar{Y}_{l0}\left(\frac{\pi}{2}, 0\right) - a[l(l+1)]^{1/2}\right.$$

$$\left.\left.\cdot\bar{Y}_{l0}\left(\frac{\pi}{2}, 0\right)\right\} x_0\,(x_0 - 1)\, F\left(l+2, 1-l, 2; x_0\right)\right],$$

$$E_a = 0, \; E_b = \frac{1}{2}e. \tag{6.13}$$

Where again for a charged ring we set $\alpha_{lm}^R \beta_{lm}^R$ zero, for current loop with no charge we set $e = 0$ and for a current loop we charge we take the full solution. The field of the current loop with no charge is visualized in Fig. 6.2.
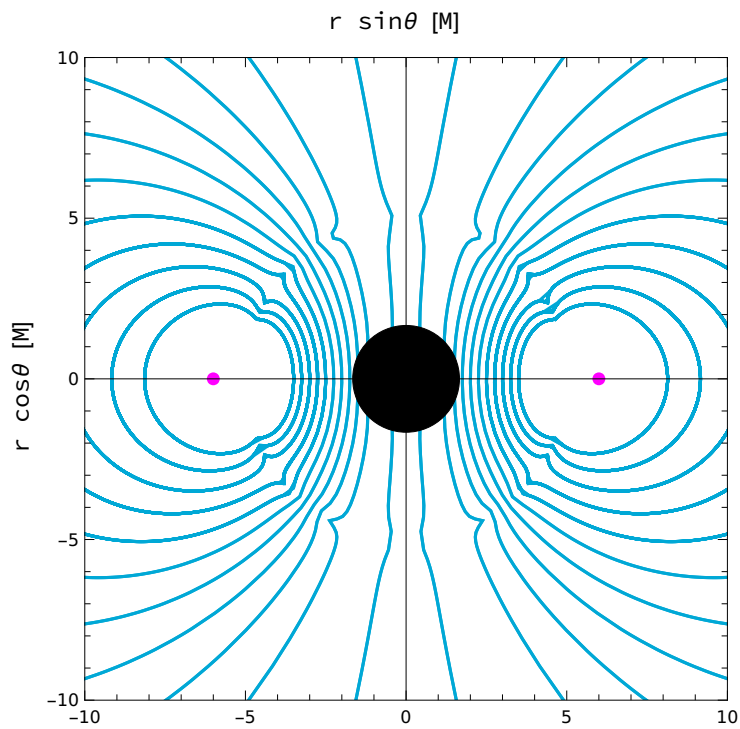
Figure 6.2: Magnetic field of axial current loop for $a = 3/4M$ located at $r = 6M$, the black hole is visualized black with the loop being magenta. At $r = 6$ we can see truncation error, we have taken first 10 l of sum.
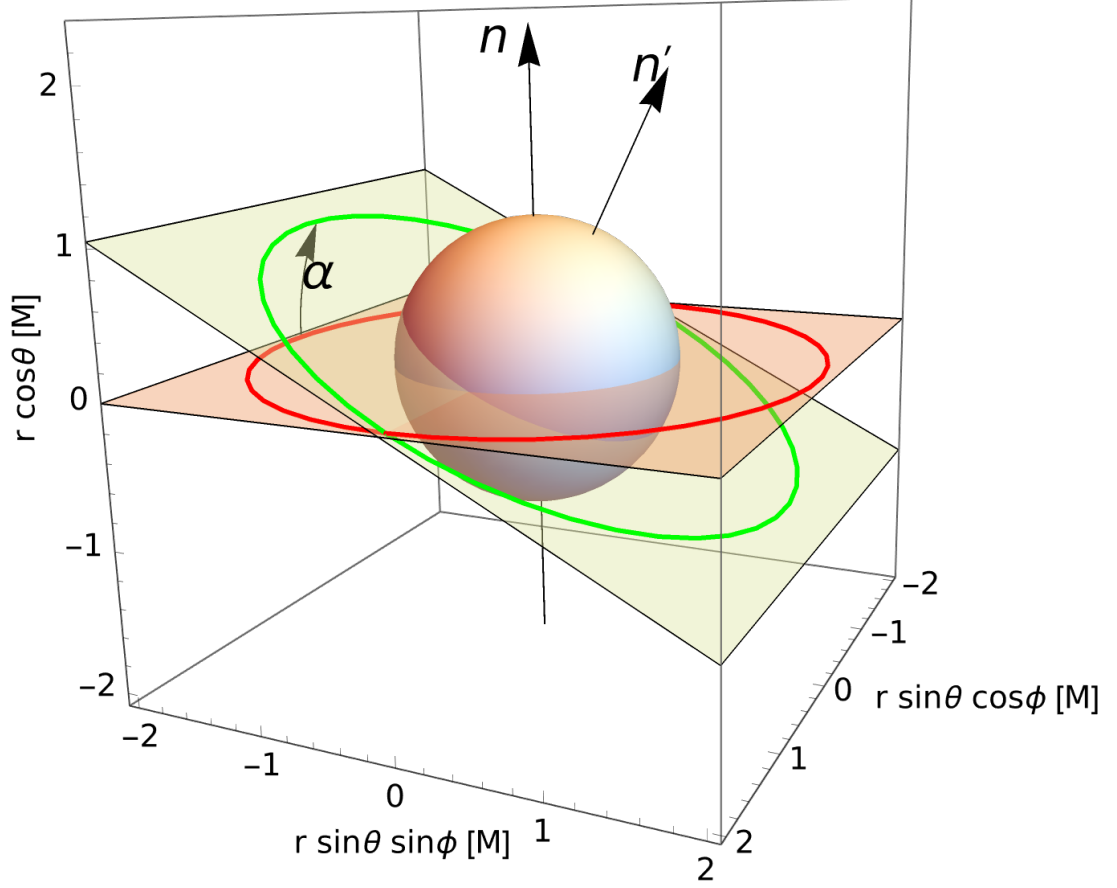
Figure 6.3: The construction of the non-axial current loop. The normal of the plane of the axial loop $n = \{0, 0, 1\}$ coincides with the axis of symmetry. The normal of the plane of the non-axial loop is denoted $n' = \{0, \Upsilon, 1\}$, the angle between the planes α. The axial loop is plotted red, the non-axial is plotted green. The parameters of the plot are $\Upsilon = 1/2$ ($\implies \alpha = 26.56°$), $r_0 = 6M$. The plot is visualized in units of Mass.

6.3 Non-axial current loop

We will now generalize the current loop above by allowing the current loop to be tilted, instead of localizing the coordinate θ to the equatorial plane $\theta = \pi/2$ we allow to loop to smoothly vary in the θ coordinate as the function of φ. We consider the ansatz

$$\mathbf{J} = (f\, \boldsymbol{\partial}_t + g\, \Upsilon \cos \varphi\, \boldsymbol{\partial}_\theta + h\, \boldsymbol{\partial}_\varphi)\, \delta(r - r_0)\delta(\theta - \frac{\pi}{2} - \Upsilon \sin \varphi). \qquad (6.14)$$

Where in general $f = f(t, \theta, \varphi), g = g(t, \theta, \varphi), h = h(t, \theta, \varphi)$, the current vector now also has a non-zero J^θ. The Υ constant symbolizes the "deflection magnitude" from the axial current loop. In reality this also defines the normal of the plane where the non-axial current loop is the coordinates $\{x = r \sin \theta cos\varphi, y = r \sin \theta \sin \varphi, z = r \cos \theta\}$ as $n^i = \{0, \Upsilon, 1\}$. To make the geometrical situation clear we have provided a visualization in (6.3). We could also parameterize by the angle between the current loop and the equatorial plane α, but the equations

43

take simpler form in the Υ parameter, these two are related by

$$\cos\alpha = \frac{1}{\sqrt{1+\Upsilon^2}}. \tag{6.15}$$

We could now directly solve the continuity equation (6.1) while correctly handling the Dirac deltas as distribution and introducing test function $L^2(\mathrm{R})$. A more elegant approach is inducing a metric on the current loop and solving the continuity equation there, we denote the induced metric by $\mathbf{g}$.

$$\mathbf{g} = \boldsymbol{g}_{|\{r=r_0,\theta=\pi/2+\Upsilon\sin\varphi\}}, \tag{6.16}$$

this metric works out to be

$$\mathbf{g} = (-1+\frac{2Mr_0}{\tilde{\Sigma}})\mathbf{d}t^2 - \frac{Mra\sin(\tilde{\theta})}{\tilde{\Sigma}}\mathbf{d}t\mathbf{d}\varphi \\ + \Upsilon^2\tilde{\Sigma}\cos^2\varphi + \sin^2(\tilde{\theta})\left(r_0+a^2+\frac{2Mr_0a^2\sin^2(\tilde{\theta})}{\tilde{\Sigma}}\right)\mathbf{d}\varphi^2, \tag{6.17}$$

where $\tilde{\Sigma} = r_0^2+a^2\cos\tilde{\theta}, \tilde{\theta} = \pi/2+\Upsilon\sin\varphi$. The determinant of the induced metric is

$$\mathbf{g}_{\mathrm{det}} = \Upsilon^2\left(2Mr_0-\tilde{\Sigma}\right)\cos^2\varphi + \left(2Mr_0-r_0^2-a^2\right)\sin^2\tilde{\theta}. \tag{6.18}$$

On such a metric the induced current vector J takes the form

$$\mathsf{J} = f\boldsymbol{\partial}_t + (h+g)\boldsymbol{\partial}_\varphi = f\boldsymbol{\partial}_t + 2F\boldsymbol{\partial}_\varphi, \tag{6.19}$$

where the definition of $F = F(\varphi)$ is obvious. The continuity equation on the induced metric takes the form

$$\frac{1}{\sqrt{-\mathbf{g}}}\frac{\partial}{\partial\mathbf{x}^i}(\sqrt{-\mathbf{g}}\,\mathsf{J}^i) = 0, \tag{6.20}$$

where $\mathbf{x}^i = \{t,\varphi\}$. Working out this equation explicitly at $\Upsilon = 0$ we get

$$f = const, \tag{6.21}$$

and

$$\frac{F'(\varphi)}{F(\varphi)} = \frac{\tilde{\theta}'(\varphi)\left(a^2\sin(2\tilde{\theta}(\varphi))\right)\left(\Delta-a^2\tilde{\theta}'(\varphi)^2\right)+2\left(a^2\Delta-a^4+(r_0^2-\Sigma)^2\right)\tilde{\theta}''(\varphi)}{2a^4\sin^2\tilde{\theta}(\varphi)\tilde{\theta}'(\varphi)^2-2a^2\Delta\left(\sin^2(\tilde{\theta}(\varphi))+\tilde{\theta}'(\varphi)^2\right)}. \tag{6.22}$$

This differential equation can be simply solved by exponentiation, denoting the right hand side of (6.22) as $\mathcal{F}(\varphi)$, we thus arrive at

$$F(\varphi) = \exp\left(\int\mathrm{d}\varphi\mathcal{F}(\varphi)\right), \tag{6.23}$$

which can be easily solved by using the substitution

$$u = 2a^4\theta'(\varphi)^2\sin^2(\theta(\varphi)) - 2a^2\Delta\left(\theta'(\varphi)^2+\sin^2(\theta(\varphi))\right), \tag{6.24}$$

finally leads to

$$F(\varphi) = \exp \int \frac{-1}{2u} \mathrm{d}u = \exp \left(-\frac{\log |u| + const}{2} \right)$$

$$= \frac{C}{\sqrt{\left| \Delta_0 \left(1 + \Upsilon^2 \left(1 + \cos(2\varphi) \right) + \cos(2\Upsilon \sin \varphi) \right) - 2\Upsilon^2 a^2 \cos^2 \varphi \cos^2(\Upsilon \sin \varphi) \right|}}.$$

$$(6.25)$$

We here note that it is *not* physically appropriate to relate the constant to the ZAMO observers, since they do not measure such a loop naturally, this only makes sense in the case of zero tilt, where the constants take for form $A = q/(2\pi\Sigma_0), C = r_0^{-1}\sqrt{\Delta_0} \left(Maq/(\pi A_0) + I\sqrt{\Delta_0/A_0} \right)$. Constructing a class of physically sensible observers which circularly orbit in the non-equatorial plane at a constant radius is not feasible, since such orbits experience precession [27]. To provide a intuitive insight, we plot the behaviour of the function $F(\varphi)$ in (6.5). The final source terms thus takes the form

$$\mathbf{J} = \left(f\boldsymbol{\partial}_t + F(\varphi)\Upsilon \cos \varphi \boldsymbol{\partial}_\theta + F(\varphi)\boldsymbol{\partial}_\varphi \right) \delta(r - r_0)\delta(\theta - \pi/2 - \mathtt{M} \sin \varphi), \quad (6.26)$$

where $f = conts$. Finally, we should now calculate the $^2 J_{lm}$ from the current vector (6.26) but we weren't able to do the integral over φ analytically, for any following graphs and results we've calculated the constants α_{lm} and β_{lm} numerically.

We can now repeat the procedure of finding integral of the eigenvalue Λ, this is shown in the Fig. 6.6. It is clear that the Meissner effect holds for such a solution. In the graph we can see that the Λ is not constant in the parameter Υ for $a = 0$ this is because we have taken the constant C to unity for each Υ. But in reality it is clear that the constant must be dependent on the parameter Υ in such a ways that for $\Upsilon \to 0$ we recover the axial current loop.

The full 3D field line plots of non-axial field can be hard to read even in the simplest case of homogeneous field. We resolved to visualizing the vector field instead. Choosing a full 3D plot, we've visualized the vector field on a center cut sphere, see Fig. 6.4.
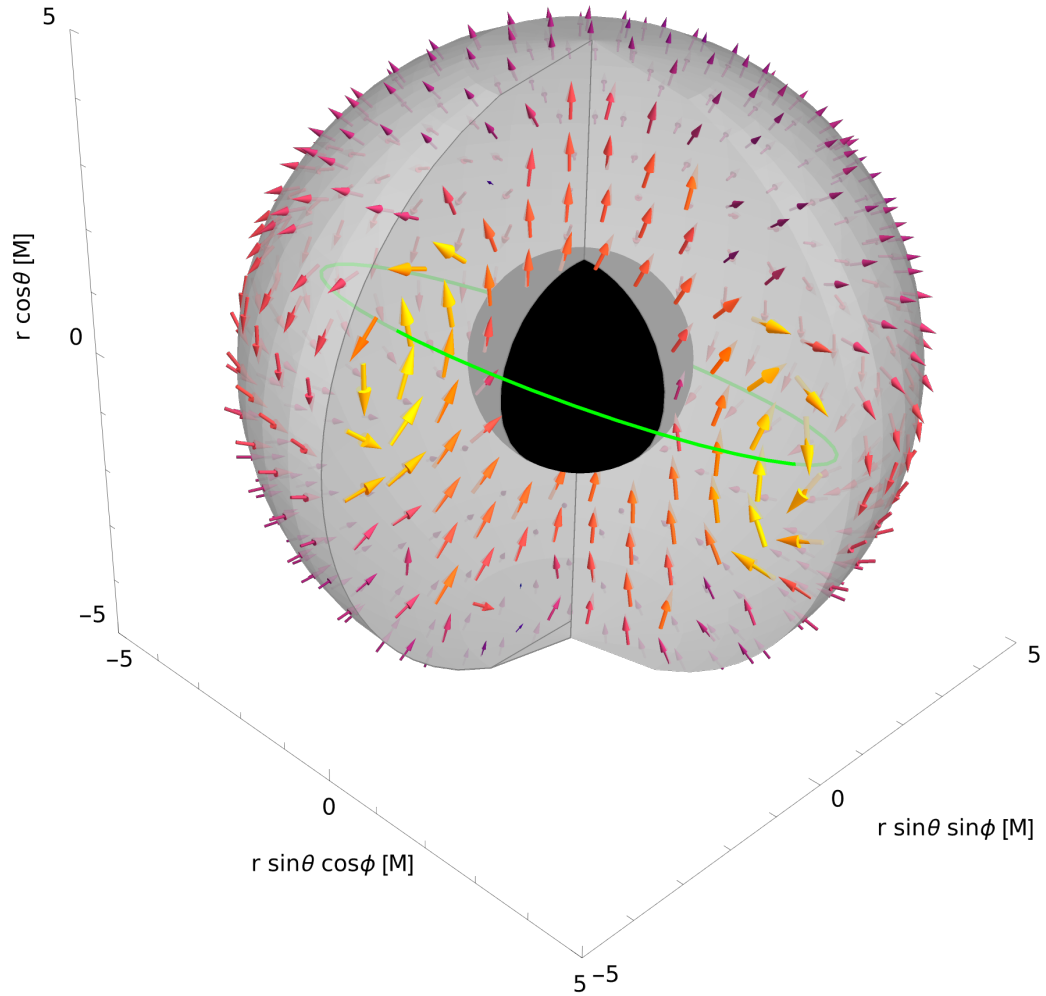
Figure 6.4: The ZAMO magnetic vector field of non-axial current loop. The parameters of the plot are $l_{max} = 7$, $\Upsilon = 1/3$, $a = 3/4M$, $r_0 = 4M$. The black hole is visualized black, the current loop is visualized green. The vector sizes as well as their color correspond to their magintudes with logarithmic scaling
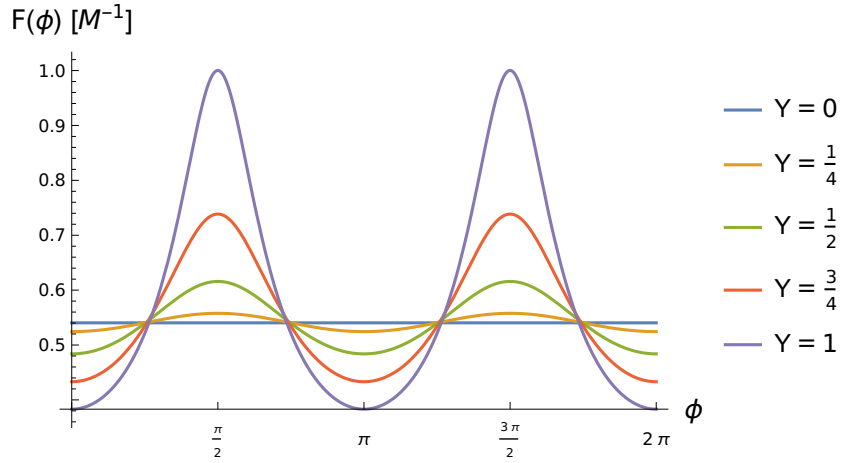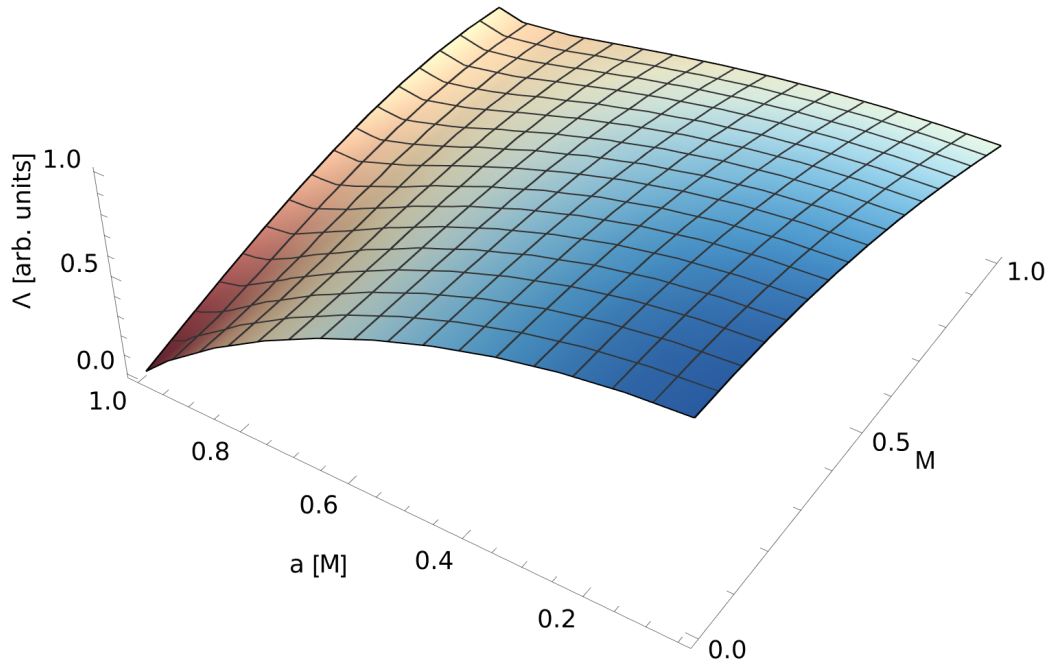
Figure 6.5: Behaviour of the $F(\varphi)$ for different Υ for $a = 1/2M$.

Figure 6.6: The Λ invariant of the non-axial current loop. The constant C was taken such that the plot is normalized to 1 at $\Upsilon = 0, a = 0$

6.4 Field of a current disk

Lastly we will reformulate the work of Vlasáková [28] in the NP formalism, where she modeled a field of a current disk. We will generalize the work by considering non-zero rotational parameter a but we will not consider a continuous current profile rather modeling the disk by superposing multiple current loops.

Consider a current loop located some distance r_n with the current I_n, we can then model a disk located between $r_0 = r_{01}$ and $r_n = r_{02}$ as having the four-current

$$J_{\text{disk}}^a = \sum_{n=1}^{N} J_{\text{loop}}^a(r_n, I_n) \tag{6.27}$$

By the linearity of Maxwell equations we can infer

$$\phi_i = \sum_{n=1}^{N} \phi_i^n, \quad i = 0, 1, 2. \tag{6.28}$$

the sum above is more of a symbolic representation, we need to note that our solutions are split into the inner and outer solution,

$$\phi_i^n = \begin{cases} \phi_i^{(I)n}, & r < r_n \\ \phi_i^{(II)n}, & r_n < r \end{cases}, \quad i = 0, 1, 2. \tag{6.29}$$

For a continuous current profile the sum goes over to the integral

$$\phi_i = \int_{r_0}^{r_N} \phi_i(\tilde{r}, I(\tilde{r})) \mathrm{d}\tilde{r}, \quad i = 0, 1, 2. \tag{6.30}$$

It is not clear what radial profile of current $I(r)$ should be, so we consider multiple possible profiles which can be seen in 6.7.

We finally provide plots of the behaviour of $B_{(r)}$ in Fig. 6.9 and $B_{(\theta)}$ in Fig. 6.10 as functions of r. We can see that the non-zero value of a changes the behaviour of such field significantly.

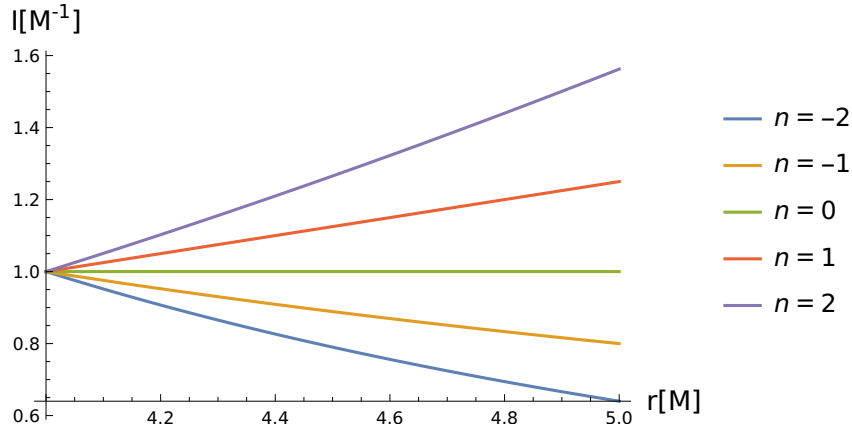$$I(r) = \left(\frac{r}{r_N}\right)^n M^{-1} \tag{6.31}$$

Figure 6.7: Radial current profile for disk located between $r = 4M$ and $r = 5M$
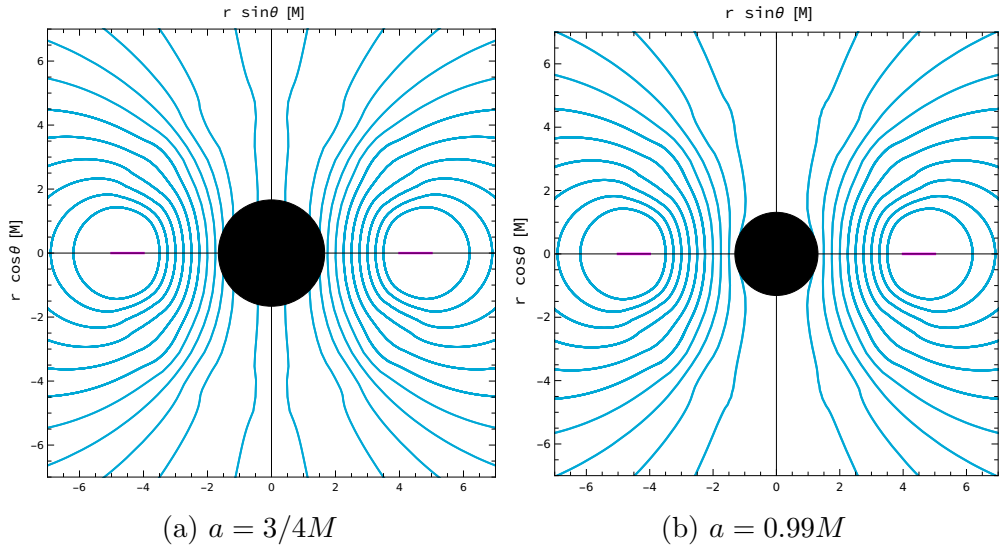
(a) $a = 3/4M$ (b) $a = 0.99M$

Figure 6.8: Magnetic field of disk using 5 loops between $r_0 = 4M$ and $r_5 = 5M$ with constant current $I(r) = I$, the disk is plotted magenta, the horizon r_+ is visualized black
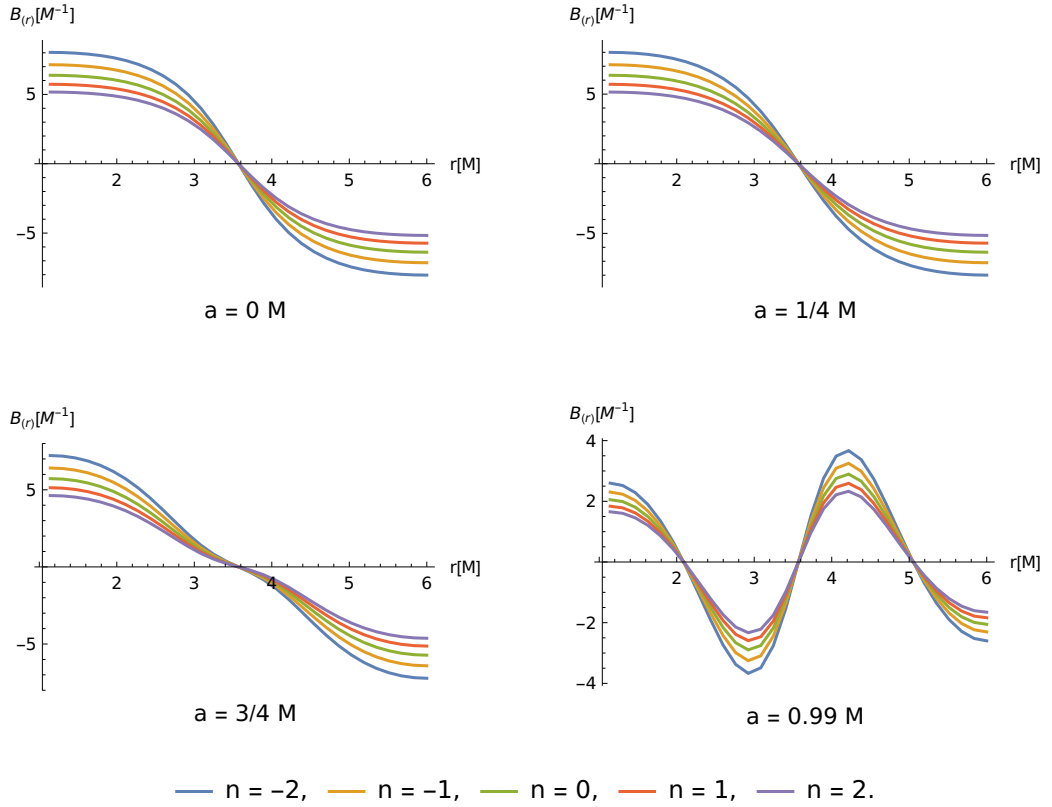

Figure 6.9: Behaviour of the radial field $B_{(r)}$ on the outer horizon $r = r_+$. The difference between the $a = 0$ case and other can be easily explained by considering that the outer horizon isn't a spherical but a quasi spherical.
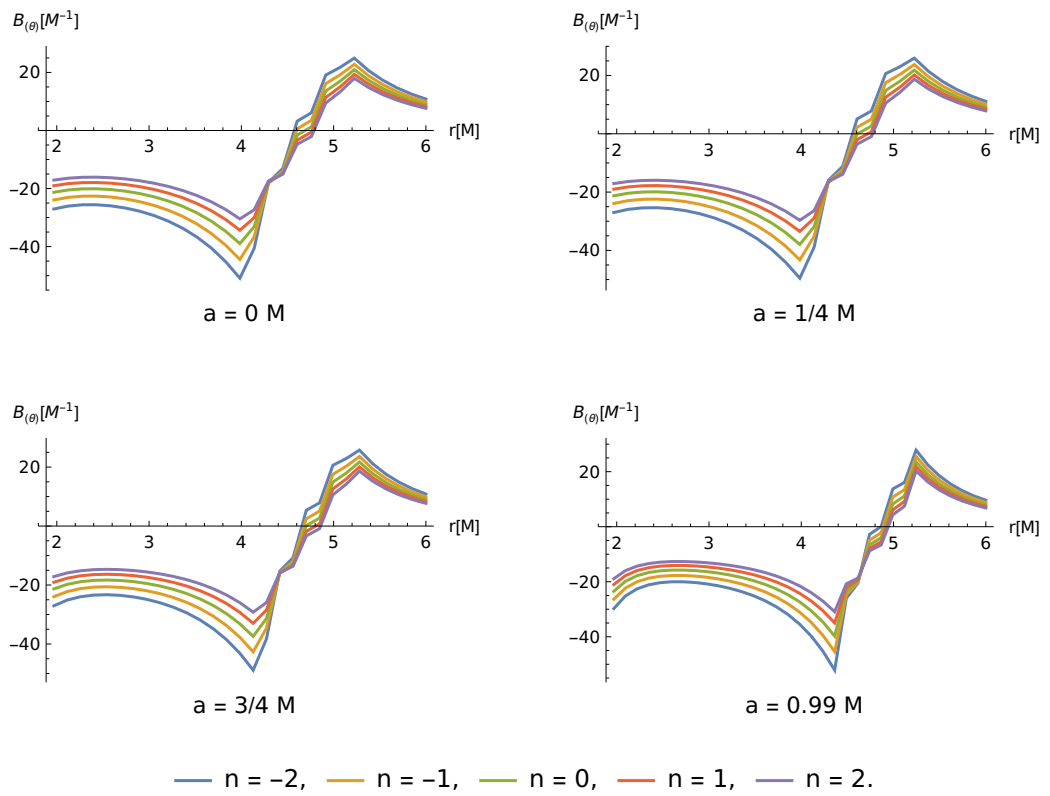
49

Figure 6.10: Behaviour of $B_{(\theta)}$ at $\theta = \pi/2$, the "bumps" are where the loops are located.

7. Magnetic fluxes

In this final section we will follow the article [10]. Which discusses the magnetic fluxes around general hemispheres of the Kerr black hole. In the extremal case $a = M$ we will find the hemisphere of maximal magnetic flux for the homogeneous magnetic field and compare this results with numerical results for the non-axial current loop.

Let us first discuss the derivation of the Eq. (4.48). Consider the tensor

$$
\mathrm{d}\sigma^{\alpha\beta} = 2\mathrm{d}x_1^{[\alpha}dx_2^{\beta]},
$$
$$
\mathrm{d}x_1^\alpha = \{0, 0, \mathrm{d}\theta, 0\}, \quad \mathrm{d}x_2^\beta = \{0, 0, 0, \mathrm{d}\varphi\}.
\tag{7.1}
$$

where [ ] denotes anti-symmetrization. Such a tensor enables one to define the surface of a black hole invariantly. Surface element of the black-hole is then

$$
\mathrm{d}S = \sqrt{\left|\frac{1}{2}\mathrm{d}\sigma_{ab}\mathrm{d}\sigma^{ab}\right|}\Big|_{r=r_+} = \sqrt{A_+}\sin\theta\mathrm{d}\theta\mathrm{d}\varphi = (r_+^2 + a^2)\sin\theta\mathrm{d}\theta\mathrm{d}\varphi.
\tag{7.2}
$$

Identical results comes when transforming the quantities in general coordinates. The total area of a black hole $\mathcal{A}$ is

$$
\mathcal{A} = \int_0^\pi \int_0^{2\pi} \mathrm{d}S = 4\pi(r^2 + a^2).
\tag{7.3}
$$

Consider now the electromagnetic field $F_{\alpha\beta}$ and it's dual $\star F_{ab}$ and some arbitrary 3-volume with the volume 3-form $\mathrm{d}\Xi_t$ and with the surface $\partial\Xi$ with the surface 2-norm $\mathrm{d}\star\xi_{ab}$. We can utilize the Gauss theorem to define appropriate fluxes. For the electric charges we have

$$
\oint_{\partial\Xi} F^{ab}\,\mathrm{d}\star\xi_{ab} = \oint_{\partial\Xi} \star F_{ab}\,\mathrm{d}\xi^{ab} = \int_\Xi 2F^{ta}{}_{;a}\,\mathrm{d}\Xi_t.
\tag{7.4}
$$

And for the "magnetic charges" we get

$$
\oint_{\partial\Xi} \star F^{ab}\,\mathrm{d}\star\xi_{ab} = \oint_{\partial\Xi} F_{ab}\,\mathrm{d}\xi^{ab} = \int_\Xi 2\star F^{ta}{}_{;a}\,\mathrm{d}\Xi_t = 0.
\tag{7.5}
$$

Thus the magnetic Φ_m and electric Φ_e flux across any surface (non-necessarily closed) is given by

$$
\Phi_m = \int_{\partial\Xi} F_{ab}\,\mathrm{d}x^a \wedge \mathrm{d}x^b, \quad \Phi_e = \int_{\partial\Xi} \star F_{ab}\,\mathrm{d}x^a \wedge \mathrm{d}x^b.
\tag{7.6}
$$

Where $\wedge$ denotes the exterior product. As already noted in Sec. 4.2 we can write this in terms of a single complex quantity (4.48). Consequently, if the the area is part of the horizon of the black hole S we get

$$
\Phi_m = \int_S F_{\theta\varphi}\,\mathrm{d}\theta\mathrm{d}\varphi, \quad \Phi_e = \int_S \star F_{\theta\varphi}\,\mathrm{d}\theta\mathrm{d}\varphi.
\tag{7.7}
$$

In [10] the integral was derived for arbitrary hemisphere.

7.1 Hemispheres of maximal flux for the extremal Black hole

In this section we will consider only the extremal black hole $a = M$, while setting the mass of the black hole to unity $M = 1$. Since an flux of arbitrary axisymmetric (part) field is zero, the hemisphere of maximal flux will always be such, that it's axis of symmetry lies in the equatorial plane. All such hemispheres can be parameterized by a single angle $\beta \in \langle -\pi, \pi \rangle$. Thus the integrals (7.7) reduce to

$$\Phi_m = \int_{\beta-\pi/2}^{\beta+\pi/2} \int_0^\pi F_{\theta\varphi} \, \mathrm{d}\theta\mathrm{d}\varphi, \quad \Phi_e = \int_{\beta-\pi/2}^{\beta+\pi/2} \int_0^\pi \star F_{\theta\varphi} \, \mathrm{d}\theta\mathrm{d}\varphi. \tag{7.8}$$

Let us now consider an arbitrary field that is homogeneous at infinity any such field will have non-zero only the terms with $l = 1$. We can integrate the field explicitly for arbitrary α_{1m} we get

$$\begin{aligned}
\Phi_m|_{l=1} &= \int_{\beta-\pi/2}^{\beta+\pi/2} \int_0^\pi F_{\theta\varphi}|_{l=1} \, \mathrm{d}\theta\mathrm{d}\varphi \\
&= \sqrt{\frac{3\pi}{8}} \left[\cos\beta \left((1+2i)\bar{\alpha}_{1-1} - (1-2i)\bar{\alpha}_{11} + (-1+2i)\alpha_{1-1} + (1+2i)\alpha_{11} \right) \right. \\
&\quad \left. + \sin(\beta) \left((1+2i)\bar{\alpha}_{1-1} + (1-2i)\bar{\alpha}_{11} + (1-2i)\alpha_{1-1} + (1+2i)\alpha_{11} \right) \right].
\end{aligned} \tag{7.9}$$

We've provided the expression in such a form, to emphasize that no terms a_{10}, this is actually the general case for every l. In the case of the field of the homogeneous field derived in the section 5.1 this reduces to

$$\Phi_m^{\text{hom.}} = \pi B_1 (\cos\beta - 2\sin\beta), \tag{7.10}$$

this result matches with the results of [10] and can be derived for arbitrary $a < M$ and M, the full expression reads

$$\Phi_m^{\text{hom.}} = \pi B_1 \left(r_+^2 \cos\beta - \left(r_+^2 + M^2 \right) a \sin\beta \right). \tag{7.11}$$

For $B_1 > 0$ this has the extrema at the points

$$\begin{aligned}
\beta_{max}^{\text{hom.}} &= -\arctan 2, \\
\beta_{min}^{\text{hom.}} &= \pi - \arctan 2,
\end{aligned} \tag{7.12}$$

which we have determined by the second derivative test, but from the geometry of the problem it's obvious that the minimum will be located at $\pi - \beta_{max}$.

Let us now repeat the procedure for the non-axial current loop. Here we need to be careful with convergence, taking $l = 16$ and the loop radius $r = 10M$, we can derive the equations for of flux (7.8) for arbitrary constants α_{lm} analytically although the expression is too long to provide here, we then substitute numerically calculated components α_{lm} of the non-axial current loop. Deriving this equation, numerically solving the equation for the extrema and then checking if we are at maxima or minima with the second derivative test we arrive at the of at a list of β indexed by the values of Υ where the flux is maximal. The variance of this list is of the order 10^{-7} with the mean value being

$$\beta_{max}^{\text{loop}} = -2.6755. \tag{7.13}$$

(a) Homogeneous field directed in $x = r \sin \theta \cos \phi$.

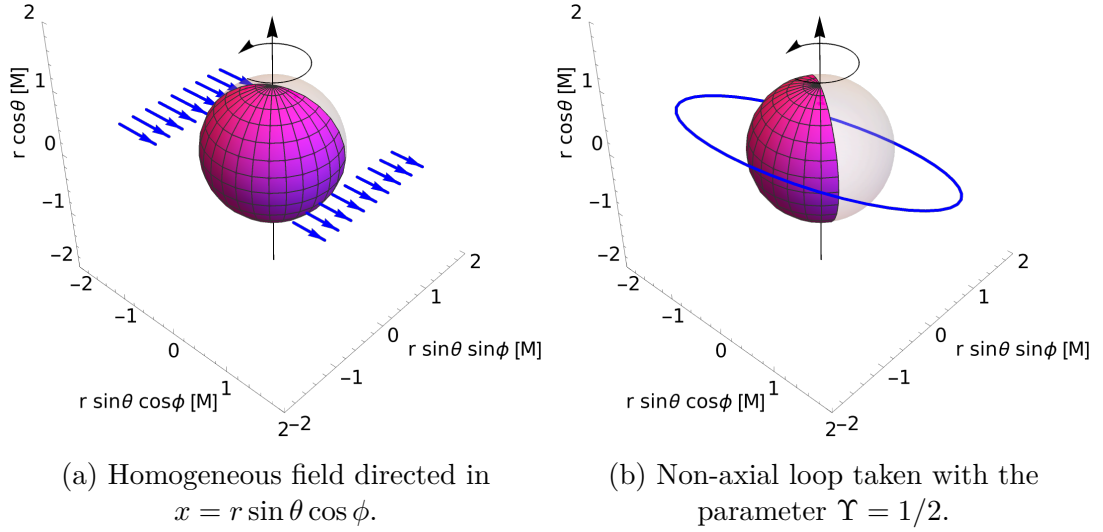(b) Non-axial loop taken with the parameter $\Upsilon = 1/2$.

Figure 7.1: 2 Visualizations of hemispheres of maximal flux. The hemispheres are colored magenta. The extremal black hole is visualized opaque. (a) the homogeneous magnetic field is visualized blue, (b) the non-axial current loop is visualized blue.

The difference of the angles between the loop and the homogeneous field is

$$\beta_{max}^{\text{loop}} - \beta_{max}^{\text{hom}} = -2.6755 + (\arctan 2) \doteq -\frac{\pi}{2}, \tag{7.14}$$

where the absolute error such a results is 0.002. The result can be intuitively understood, we vary the loop of the direction of $y = r \sin \theta \sin \varphi$, but the homogeneous magnetic field has the direction $x = r \sin \theta \cos \varphi$, thus the maximal hemispheres are only shifted by 90°. It is not quite clear why the hemispheres should be the same (expect for the shift $\pi/2$), because the field are very differently even for the extremal case. We also want to note that we've received the same result when varying varying the loop diameter from $r_0 = 40$ to $r_0 = 4$. For lower values of $r \leq 4$ we've run into more problems with numerical calculations and the error grew (although the error was not larger than 0.05). It could be possible that the non-circular profile of the loop located near the horizon causes the hemisphere to shift slightly, but as we've already said, we suspect that this was just a numerical error of the calculations.

Conclusion

This thesis explored the application of NP formalism for the Kerr spacetime. We've built upon the work of prof. Bičák who derived the solution for arbitrary stationary electromagnetic test field. Using these results, we identified the source term and the associated electromagnetic field of a non-axial current loop.

Further we analyzed the solution by calculating the electromagnetic invariant (eigenvalue of the associated energy momentum tensor) on the horizon. Revealing expected behaviour but also showing possible problems with the solution.

We've also explored the Meissner effect, providing full mathematical proof in the Kerr spacetime. Notably we noticed that not only the flux of arbitrary stationary axially symmetric electromagnetic field across the extremal black hole vanishes but also that both of electromagnetic invariants vanish. We then discussed different possible visualization techniques of the electromagnetic field lines, these visualizations revealed a surprising diversity of configurations.

Finally, we determined the hemisphere of maximal flux for the non-axial loop. And shown, how this is related to the known hemisphere of maximal flux for the homogeneous magnetic field.

Bibliography

[1] C. Yuzhu, K. Hada, T. Kawashima, M. Kino, W. Lin, M. Honma, H. Ro, Y. Mizuno, K. Yi, J. Yu, J. Park, W. Jiang, Z.-Q. Shen, E. Kravchenko, J. Algaba, X. Cheng, I. Cho, G. Giovannini, M. Giroletti, and W. Zhong, "Precessing jet nozzle connecting to a spinning black hole in M87," feb 2023.

[2] J. Bičák and L. Dvořák, "Stationary electromagnetic fields around black holes. II. general solutions and the fields of some special sources near a Kerr black hole," vol. 7, pp. 959–983, dec 1976.

[3] M. Visser, "The Kerr spacetime: A brief introduction," *arXiv, doi: arXiv:0706.0622*, 2008.

[4] J. B. Griffiths and J. Podolský, *Exact Space-Times in Einstein's General Relativity*. Cambridge Monographs on Mathematical Physics, Cambridge University Press, 2009.

[5] C. Doran, "New form of the Kerr solution," *Physical Review D*, vol. 61, Feb. 2000.

[6] N. A. Sharp, "On embedding of the Kerr geometry.," *Canadian Journal of Physics*, vol. 59, pp. 688–692, May 1981.

[7] G. W. Gibbons, C. A. R. Herdeiro, and C. Rebelo, "Global embedding of the Kerr black hole event horizon into hyperbolic 3-space," *Phys. Rev. D*, vol. 80, p. 044014, Aug 2009.

[8] S. Chandrasekhar, *The Mathematical Theory of Black Holes*, pp. 5–26. Dordrecht: Springer Netherlands, 1984.

[9] O. Semerák and J. Bičák, *Relativistic Physics, lecture notes for a course taught at Prague math-phys.* 2023.

[10] J. Bičák and V. Janiš, "Magnetic fluxes across black holes," vol. 212, pp. 899–915, feb 1985. ADS Bibcode: 1985MNRAS.212..899B.

[11] E. Newman and R. Penrose, "An Approach to Gravitational Radiation by a Method of Spin Coefficients," *Journal of Mathematical Physics*, vol. 3, pp. 566–578, May 1962.

[12] J. N. Goldberg and R. K. Sachs, "A theorem on Petrov types," *Acta Physica Polonica B, Proceedings Supplement*, vol. 22, p. 13, Jan. 1962.

[13] "xAct: Efficient tensor computer algebra for the Wolfram Language." `http://www.xact.es/`.

[14] L. D. Landau and E. M. Lifschits, *The Classical Theory of Fields*, vol. Volume 2 of *Course of Theoretical Physics*. Oxford: Pergamon Press, 1975.

[15] S. A. Teukolsky and W. H. Press, "Perturbations of a rotating black hole. III - interaction of the hole with gravitational and electromagnetic radiation," vol. 193, p. 443.

[16] "*NIST Digital Library of Mathematical Functions.*" `https://dlmf.nist.gov/`, Release 1.2.0 of 2024-03-15. F. W. J. Olver, A. B. Olde Daalhuis, D. W. Lozier, B. I. Schneider, R. F. Boisvert, C. W. Clark, B. R. Miller, B. V. Saunders, H. S. Cohl, and M. A. McClain, eds.

[17] D. Kofroň, "Point particles and appell's solutions on the axis of Kerr black hole for arbitrary spin in terms of the Debye potentials," vol. 101, p. 064027, mar 2020.

[18] W. Meissner and R. Ochsenfeld, "Ein neuer effekt bei eintritt der supraleitfhigkeit," vol. 21, pp. 787–788, nov.

[19] R. M. Wald, "Black hole in a uniform magnetic field," *Phys. Rev. D*, vol. 10, pp. 1680–1685, Sep 1974.

[20] A. R. King, J. P. Lasota, and W. Kundt, "Black holes and magnetic fields," *Phys. Rev. D*, vol. 12, pp. 3037–3042, Nov 1975.

[21] S. S. Komissarov and J. C. McKinney, "The 'Meissner effect' and the Blandford—Znajek mechanism in conductive black hole magnetospheres," *Monthly Notices of the Royal Astronomical Society: Letters*, vol. 377, p. L49–L53, May 2007.

[22] J. Bičák and T. Ledvinka, "Electromagnetic fields around black holes and Meissner effect," 2000.

[23] R. F. Penna, "Black hole Meissner effect and blandford-znajek jets," *Physical Review D*, vol. 89, May 2014.

[24] J. Bičák, V. Karas, and T. Ledvinka, "Black holes and magnetic fields," *Proceedings of the International Astronomical Union*, vol. 2, no. S238, p. 139–144, 2006.

[25] F. Hejda and J. Bičák, "Extremal black holes in strong magnetic fields: Near-horizon geometries and Meissner effect," in *The Fourteenth Marcel Grossmann Meeting*, WORLD SCIENTIFIC, Nov. 2017.

[26] Z. Budinova, M. Dovčiak, V. Karas, and A. Lanza, "Magnetic fields around black holes," *European Journal of Physics*, vol. 21, 06 2000.

[27] A. Al Zahrani, "Tilted circular orbits around a Kerr black hole," *Physical Review D*, vol. 109, Jan. 2024.

[28] Z. Vlasáková, "Pole proudových smyček kolem černých děr," master's thesis, Univerzita Karlova, 2020.

[29] J. N. Goldberg, A. J. Macfarlane, E. T. Newman, F. Rohrlich, and E. C. G. Sudarshan, "Spin-s Spherical Harmonics and ," *Journal of Mathematical Physics*, vol. 8, pp. 2155–2161, Nov. 1967.

[30] R. Geroch, A. Held, and R. Penrose, "A space-time calculus based on pairs of null directions," *Journal of Mathematical Physics*, vol. 14, pp. 874–881, July 1973.

[31] "Black Hole Perturbation Toolkit." (bhptoolkit.org).

A. Appendix

A.1 Spin Weighted Spherical Harmonics

We will follow the article [29], where they in detail describe the spin-weighted spherical harmonics. The spin-weighted spherical harmonics represent the spherical harmonics with additional s that represents the $U(1)$ symmetry. First we consider the three dimensional Euclidian space with the coordiantes $\{r, \theta, \phi\}$ and introduce the orthonormal triad $\mathbf{a}, \mathbf{b}, \mathbf{c}$, where $\mathbf{c}$ points in the radial direction and $\mathbf{a}, \mathbf{b}$ are tangent to a sphere of radius r. We complexify the triad by introducing the complex vector $\mathbf{m}$ and it's complex conjugate $\overline{\mathbf{m}}$

$$\sqrt{2}\mathbf{m} = \mathbf{a} + i\mathbf{b}. \tag{A.1}$$

Of course $\mathbf{a}$ and $\mathbf{b}$ were defined up to a rotation angle ψ so that now $\mathbf{m}$ and $\overline{\mathbf{m}}$ are defined up to a phase $\mathbf{m}' = e^{i\psi}\mathbf{m}$. We're now able to define the spin-weight s, we say that a quantity η is of the spin-weight s if it transform under the rotation angle ψ as

$$\eta' = e^{is\psi}\eta. \tag{A.2}$$

From this we can, for example see, that the vector $\mathbf{c}$ is of the spin-weight 0 since it does not change under the rotation. We will now introduce the $\eth$ operator, such operator is not important only in deriving spin-weighted spherical harmonics, but in a whole tetrad formalism in GR called the GHP (Geroch, Held, Penrose) formalism [30], which is a special form of the NP formalism already introduced. Here we simplify define the $\eth$ operator by it's action on a quantity η with the s

$$\eth\eta = -(\sin\theta)^s \left[\frac{\partial}{\partial\theta} + \frac{i}{\sin\theta}\frac{\partial}{\partial\phi}\right](\sin\theta)^{-s}\eta, \tag{A.3}$$

which implies that the $\eth$ operator raises the spin-weight by 1 since

$$(\eth\eta)' = e^{i(s+1)\psi}(\eth\eta). \tag{A.4}$$

In the same sense one can define the conjugate operator $\overline{\eth}$

$$\eth\eta = -(\sin\theta)^s \left[\frac{\partial}{\partial\theta} - \frac{i}{\sin\theta}\frac{\partial}{\partial\phi}\right](\sin\theta)^{-s}\eta, \tag{A.5}$$

which lowers the spin-weight by one

$$(\overline{\eth}\eta)' = e^{i(s-1)\psi}(\overline{\eth}\eta). \tag{A.6}$$

Consider now the ordinary spherical-harmonics $Y_{lm}(\theta, \phi)$ we can define the spin-weighted spherical harmonics $_sY_{lm}(\theta, \phi)$ by

$$_sY_{lm}(\theta, \phi) = \begin{cases} \sqrt{\frac{(l-s)!}{(l+s)!}}\, \eth^s Y_{lm}(\theta, \phi) & 0 \le s \le l, \\ \sqrt{\frac{(l+s)!}{(l-s)!}}\left(-\overline{\eth}\right)^{-s} Y_{lm}(\theta, \phi) & -l \le s \le 0. \end{cases} \tag{A.7}$$

Spin-wieghted spherical harmonics are undefined for $|s| > l$. Explicitly these can be written as

$$\begin{aligned}
_sY_{lm}(\theta, \phi) &= \sqrt{\frac{(l+m)!(l-m)!}{(l+s)!(l-s)!}\frac{2l+1}{4\pi}}(\sin\theta/2)^{2l} \\
&\quad \cdot \sum_k \binom{l-s}{k}\binom{l+s}{k+s-m}(-1)^{1-k-s}e^{im\phi}(\cot\theta/2)^{2k+s-m}.
\end{aligned} \tag{A.8}$$

Such spin-wieghted spherical harmonics form a complete orthonormal set for each value of s. That is any spin-wieghted function of the wight s can be expanded into such a series of $_sY_{lm}(\theta\phi)$. Finally we note that the spin-weighted spherical harmonics have been numerically implement in the Mathematica package Black hole pertubation toolkit [31], which we have used for the numeric calculations.

A.2   Maxwell tensor and it's projection

Since in the text we provided the forms of the NP quantites $\varphi_0, \varphi_1, \varphi_2$ we will here provide the whole Maxwell tensor along with the projection of the self dual form 3.6 to the ZAMO **u** and Doran **ũ** four velocities and their appropriate tetrad projections in the Boyer-lindquist coordiantes 1.5.

First the tensor **F** has the components in the Boyer-Lindquist coordiantes

$$\begin{aligned}
F_{tr} &= -\varphi_1 + \frac{ia\varphi_0\sin\theta}{\sqrt{2}(2-4r)} - \frac{ia\varphi_2(\overline{\varrho}-2r)\sin\theta}{\sqrt{2}\Delta} + c.c. \\
F_{t\theta} &= -\frac{\Sigma\varphi_2}{\sqrt{2}\overline{\varrho}} - \frac{\Delta\varphi_0}{\sqrt{2}(2\overline{\varrho}-4r)} - ia\varphi_1\sin\theta + c.c. \\
F_{t\phi} &= \frac{i\Delta\varphi_0\sin\theta}{\sqrt{2}(2\overline{\varrho}-4r)} + \frac{i}{\sqrt{2}}\varphi_2(\overline{\varrho}-2r)\sin\theta + c.c. \\
F_{r\theta} &= \frac{1}{2\sqrt{2}}\overline{\varrho}\varphi_0 - \frac{\Sigma\varphi_2(\overline{\varrho}-2r)}{\sqrt{2}\Delta} + c.c. \\
F_{r\phi} &= \frac{i\varphi_0(\Delta+2Mr)\sin\theta}{2\sqrt{2}(\overline{\varrho}-2r)} - \frac{i\varphi_2(\overline{\varrho}-2r)(\Delta+2Mr)\sin\theta}{\sqrt{2}\Delta} - a\varphi_1\sin^2\theta + c.c. \\
F_{\theta\phi} &= -i\varphi_1(\Delta+2Mr)\sin\theta + \frac{a\Delta\overline{\varrho}\varphi_0\sin^2\theta}{2\sqrt{2}\Sigma} + \frac{1}{\sqrt{2}}a\varphi_2(\overline{\varrho}-2r)\sin^2\theta + c.c.
\end{aligned} \tag{A.9}$$

where *c.c.* denotes the complex conjugate. Then we denote the projection of the self-dual form to the four-velocity of the ZAMO observer as $\mathcal{E}^a = {}^*F^{ba}u_a$ is

$$\begin{aligned}
\mathcal{E}^t &= 0, \\
\mathcal{E}^r &= -\frac{2\Delta^{1/2}\Sigma^{1/2}\varphi_1}{A^{1/2}} - \frac{ia\Delta^{1/2}\Sigma^{1/2}\varphi_0\sin\theta}{\sqrt{2}A^{1/2}\varrho} + \frac{i\sqrt{2}a\varrho\Sigma^{1/2}\varphi_2\sin\theta}{A^{1/2}\Delta^{1/2}}, \\
\mathcal{E}^\theta &= \frac{\Delta^{3/2}\Sigma^{1/2}\varphi_0}{\sqrt{2}A^{1/2}\varrho} - \frac{\sqrt{2}\Delta^{1/2}\varrho\Sigma^{1/2}\varphi_2}{A^{1/2}} - \frac{2ia\Delta^{1/2}\Sigma^{1/2}\varphi_1\sin\theta}{A^{1/2}}, \\
\mathcal{E}^\phi &= -\frac{i\Delta^{3/2}\Sigma^{1/2}\varphi_0\sin\theta}{\sqrt{2}A^{1/2}\varrho} - \frac{i\sqrt{2}\Delta^{1/2}\varrho\Sigma^{1/2}\varphi_2\sin\theta}{A^{1/2}}.
\end{aligned} \tag{A.10}$$

We remind the reader that (modulo sign) the electric $\mathbf{E}$ and magnetic $\mathbf{B}$ field are real and imaginary part of $\mathcal{E}$ respectively. Projecting this to the ZAMO tetrad we get

$$
\begin{aligned}
\mathcal{E}^{(t)} &= 0, \\
\mathcal{E}^{(r)} &= -\frac{2\Sigma\varphi_1}{A^{1/2}} + \frac{i\sqrt{2}a\varrho\Sigma\varphi_2\sin\theta}{A^{1/2}\Delta} + \frac{ia\varphi_0(\varrho-2r)\sin\theta}{\sqrt{2}A^{1/2}}, \\
\mathcal{E}^{(\theta)} &= -\frac{\sqrt{2}\Delta^{1/2}\varrho\Sigma\varphi2}{A^{1/2}} - \frac{\Delta^{3/2}\varphi_0(\varrho-2r)}{\sqrt{2}A^{1/2}} - \frac{2ia\Delta^{1/2}\Sigma\varphi_1\sin\theta}{A^{1/2}}, \\
\mathcal{E}^{(\phi)} &= -\frac{i\Delta^{3/2}\varphi_0\sin^2\theta}{\sqrt{2}\varrho} - i\sqrt{2}\Delta^{1/2}\varrho\varphi_2\sin^2\theta.
\end{aligned}
\tag{A.11}
$$

For the Doran tetrad we denote the projection as $\tilde{\mathcal{E}} = {}^*F^{ba}\tilde{u}_a$

$$
\begin{aligned}
\tilde{\mathcal{E}}^t &= \frac{\sqrt{Mr\,(\Delta+2Mr)}}{\Delta\Sigma^2}\left(2\sqrt{2}\Sigma\varphi_1(\Delta+2Mr) + \frac{ia\Delta\Sigma\varphi_0\sin\theta}{\varrho} + \frac{2ia\Sigma^2\varphi_2\sin\theta}{\varrho-2r}\right), \\
\tilde{\mathcal{E}}^r &= -\frac{2\varphi_1(\Delta+2Mr)}{\Sigma} - \frac{ia\Delta\varphi_0\sin\theta}{\sqrt{2}\varrho\Sigma} - \frac{i\sqrt{2}a\varphi_2\sin\theta}{\varrho-2r}, \\
\tilde{\mathcal{E}}^\theta &= \frac{\Delta\varphi_0(\Delta+2Mr)^{1/2}}{2M^{1/2}\varrho\Sigma r^{1/2} + \sqrt{2}\varrho\Sigma(\Delta+2Mr)^{1/2}} - \frac{2ia\varphi_1\sin\theta}{\Sigma} \\
&\quad + \frac{\varphi_2\left(\sqrt{2}\Delta + 2\sqrt{2}Mr + 2M^{1/2}r^{1/2}(\Delta+2Mr)^{1/2}\right)}{\Delta\varrho - 2\Delta r} \\
\tilde{\mathcal{E}}^\phi &= \frac{2\sqrt{2Mr}a\varphi_1(\Delta+2Mr)^{1/2}}{\Delta\Sigma} + \frac{i\varphi_2\csc\theta\left(\sqrt{2}\Sigma + 2M^{1/2}\,r^{1/2}(\Delta+2Mr)^{1/2}\right)}{\Delta(\varrho-2r)} \\
&\quad - \frac{i\varphi_0\left(\sqrt{2}\Sigma - 2M^{1/2}r^{1/2}(\Delta+2Mr)^{1/2}\right)}{\sin\theta 2\varrho\Sigma}.
\end{aligned}
\tag{A.12}
$$

and finally projecting to the Doran tetrad

$$
\begin{aligned}
\tilde{\mathcal{E}}^{(t)} &= 0, \\
\tilde{\mathcal{E}}^{(r)} &= \frac{(\Delta+2Mr)^{1/2}}{\Sigma^{1/2}}\left(-2\varphi_1 - \tfrac{1}{2\varrho}ia\varphi_0\left(\sqrt{2} - \frac{2M^{1/2}r^{1/2}}{(\Delta+2Mr)^{1/2}}\right)\sin\theta \right. \\
&\quad \left. \frac{ia\varrho}{\Delta}\varphi_2\left(\sqrt{2} + \frac{2M^{1/2}r^{1/2}}{(\Delta+2Mr)^{1/2}}\right)\sin\theta\right), \\
\tilde{\mathcal{E}}^{(\theta)} &= \frac{\Delta\varphi_0}{2M^{1/2}\varrho r^{1/2} + \sqrt{2}\varrho(\Delta+2Mr)^{1/2}} - \frac{2ia\varphi_1\sin\theta}{(\Delta+2Mr)^{1/2}} \\
&\quad + \frac{\varphi_2\left(2M^{1/2}\Sigma r^{1/2} + \sqrt{2}\Sigma(\Delta+2Mr)^{1/2}\right)}{\Delta\varrho - 2\Delta r}, \\
\tilde{\mathcal{E}}^{(\phi)} &= -\frac{i\Sigma^{1/2}\varphi_0\left(\sqrt{2} - \frac{2M^{1/2}r^{1/2}}{(\Delta+2Mr)^{1/2}}\right)}{2\varrho} + \frac{i\Sigma^{3/2}\varphi_2\left(\sqrt{2} + \frac{2M^{1/2}r^{1/2}}{(\Delta+2Mr)^{1/2}}\right)}{\Delta(\varrho-2r)}.
\end{aligned}
\tag{A.13}
$$